



# Phage display and kinetic selection of antibodies that specifically inhibit amyloid self-replication

Anna Munke<sup>a,1</sup>, Jonas Persson<sup>a,2</sup>, Tanja Weiffert<sup>a</sup>, Erwin De Genst<sup>b,3</sup>, Georg Meisl<sup>b</sup>, Paolo Arosio<sup>b,4</sup>, Anna Carnerup<sup>c</sup>, Christopher M. Dobson<sup>b</sup>, Michele Vendruscolo<sup>b</sup>, Tuomas P. J. Knowles<sup>b,d</sup>, and Sara Linse<sup>a,5</sup>

<sup>a</sup>Department of Biochemistry and Structural Biology, Chemical Centre, Lund University, SE221 00 Lund, Sweden; <sup>b</sup>Department of Chemistry, University of Cambridge, Cambridge CB2 1EW, United Kingdom; <sup>c</sup>Department of Physical Chemistry, Chemical Centre, Lund University, SE221 00 Lund, Sweden; and <sup>d</sup>Cavendish Laboratory, Department of Physics, University of Cambridge, Cambridge CB3 0HE, United Kingdom

Edited by James A. Wells, University of California, San Francisco, CA, and approved May 10, 2017 (received for review January 9, 2017)

**The aggregation of the amyloid  $\beta$  peptide (A $\beta$ ) into amyloid fibrils is a defining characteristic of Alzheimer's disease. Because of the complexity of this aggregation process, effective therapeutic inhibitors will need to target the specific microscopic steps that lead to the production of neurotoxic species. We introduce a strategy for generating fibril-specific antibodies that selectively suppress fibril-dependent secondary nucleation of the 42-residue form of A $\beta$  (A $\beta$ 42). We target this step because it has been shown to produce the majority of neurotoxic species during aggregation of A $\beta$ 42. Starting from large phage display libraries of single-chain antibody fragments (scFvs), the three-stage approach that we describe includes (i) selection of scFvs with high affinity for A $\beta$ 42 fibrils after removal of scFvs that bind A $\beta$ 42 in its monomeric form; (ii) ranking, by surface plasmon resonance affinity measurements, of the resulting candidate scFvs that bind to the A $\beta$ 42 fibrils; and (iii) kinetic screening and analysis to find the scFvs that inhibit selectively the fibril-catalyzed secondary nucleation process in A $\beta$ 42 aggregation. By applying this approach, we have identified four scFvs that inhibit specifically the fibril-dependent secondary nucleation process. Our method also makes it possible to discard antibodies that inhibit elongation, an important factor because the suppression of elongation does not target directly the production of toxic oligomers and may even lead to its increase. On the basis of our results, we suggest that the method described here could form the basis for rationally designed immunotherapy strategies to combat Alzheimer's and related neurodegenerative diseases.**

Alzheimer | antibody | inhibitor | drug development | self-assembly

The misfolding and aggregation of protein molecules is associated with a range of debilitating human disorders including Alzheimer's disease (AD), Parkinson's disease, and type II diabetes (1, 2). Common to these diseases are deposits of protein aggregates that proliferate and spread through the brain or other organs, processes that are currently very difficult to combat. AD leads to degeneration of neurons and synapses and is the most common form of dementia (3, 4). Several lines of evidence link the amyloid  $\beta$  peptide (A $\beta$ ) and its self-assembly reaction to AD (5–7). Monomeric A $\beta$  peptides are unstructured in solution, but oligomeric (8, 9) and fibrillar (10–13) aggregates contain a high proportion of  $\beta$ -sheet structure. Monomers and fibrils appear to be relatively harmless, whereas at least some oligomeric species have significant toxicity and are likely to be linked to neurodegeneration (14, 15).

No therapeutic approach has been shown to affect the progression of AD, although some compounds such as cholinesterase inhibitors help to manage the symptoms for a limited time. The main approaches in the search for therapies in recent years have been the development of  $\beta$ - and  $\gamma$ -secretase inhibitors and of immunotherapy (16). The first approach aims at reducing A $\beta$  production or lowering the proportion of the more toxic A $\beta$ 42 variant relative to the other isoforms. The latter strategy includes active immunization with A $\beta$  and passive immunization using anti-A $\beta$  antibodies (17). Clinical trials of antibody-based therapeutics have proved challenging and in some cases have revealed

significant complications such as adverse inflammatory reactions (18). Recent advances include the use of autoantibodies derived from elderly individuals who are cognitively normal, with some favorable indications for aggregate-specific antibody Aducanumab (19). These results generate optimism that new strategies for deriving A $\beta$  species-specific antibodies might become attractive.

Anti-A $\beta$  antibodies (*SI Appendix, Table S1*) are reported to have three main modes of action: (i) modulation of phagocytosis, (ii) alteration of the distribution of A $\beta$  between the CNS and plasma, and (iii) inhibition of aggregation through binding to A $\beta$  oligomers. Here we propose an alternative strategy aimed at deriving fibril-specific antibodies based on the idea that such antibodies may block fibril-dependent aggregation processes. Our strategy has emerged from recent advances in the understanding of the A $\beta$ 42 aggregation mechanism in vitro, with the discovery of the secondary nucleation of monomers on fibril surfaces as the major contribution to aggregate proliferation and toxicity (20, 21). Such secondary nucleation dominates the formation of new aggregates from early stages of the aggregation process and provides an autocatalytic feedback reaction, which appears to generate the

## Significance

The promise of antibody-based strategies to combat Alzheimer's disease by inhibiting the aggregation of the amyloid  $\beta$  peptide (A $\beta$ ) has not yet been realized in clinical trials. In part, this situation has arisen because the antibodies explored so far have been developed without the benefit of the mechanistic information needed to block specific steps in A $\beta$  aggregation. We introduce a strategy to target specifically fibril-dependent secondary nucleation, the microscopic step found to generate most neurotoxic A $\beta$  assemblies. Phage display libraries are screened to find antibodies that bind to A $\beta$  fibrils, followed by affinity ranking and chemical kinetic analysis. Our results suggest that such antibodies may serve as starting points for the development of effective therapeutics for neurodegenerative diseases.

Author contributions: A.M., J.P., T.W., and S.L. designed research; A.M., J.P., T.W., E.D.G., A.C., and S.L. performed research; G.M., P.A., and S.L. contributed new reagents/analytic tools; A.M., J.P., T.W., G.M., P.A., M.V., T.P.J.K., and S.L. analyzed data; and A.M., G.M., C.M.D., M.V., T.P.J.K., and S.L. wrote the paper.

The authors declare no conflict of interest.

This article is a PNAS Direct Submission.

Freely available online through the PNAS open access option.

<sup>1</sup>Present address: Laboratory of Molecular Biophysics, Department of Cell and Molecular Biology, Uppsala University, SE-75124 Uppsala, Sweden.

<sup>2</sup>Present address: Department of Immunology, Genetics and Pathology, Uppsala University, 751 85 Uppsala, Sweden.

<sup>3</sup>Present address: Innovative Medicines, Discovery Sciences, Astra Zeneca, Cambridge CB4 0WG, United Kingdom.

<sup>4</sup>Present address: Department of Chemistry and Applied Biosciences, ETH Zürich, 8093 Zurich, Switzerland.

<sup>5</sup>To whom correspondence should be addressed. Email: sara.linse@biochemistry.lu.se.

This article contains supporting information online at [www.pnas.org/lookup/suppl/doi:10.1073/pnas.1700407114/-DCSupplemental](http://www.pnas.org/lookup/suppl/doi:10.1073/pnas.1700407114/-DCSupplemental).

large majority of toxic oligomers (20–22). Inhibition of secondary nucleation can therefore lead to a dramatic decrease in the total number of oligomers formed during the aggregation process (21–24). By contrast, inhibiting the other two steps in the underlying mechanism, primary nucleation and elongation (20), will lead only to a delay in the formation of oligomers and, in the case of elongation, may increase the total quantities of these toxic species.

In a previous study, we have shown that the molecular chaperone pro-SPC Brichos inhibits secondary nucleation in a highly selective manner by binding to the fibril surfaces, thereby reducing substantially the toxicity resulting from the aggregation process (21). Inspired by the efficacy of this natural molecule in curtailing A $\beta$ 42 toxicity, we have here developed a systematic approach to the generation of single-chain antibody fragments (scFvs) that bind specifically to the fibrillar form of A $\beta$ 42. We demonstrate that this approach allows identification of antibody fragments that inhibit selectively the secondary nucleation of A $\beta$ 42 on fibril surfaces.

## Results

**Generation of ScFvs with High Affinity for A $\beta$ 42 Fibrils.** The strategy used here for deriving antibody fragments with the ability to inhibit fibril-dependent microscopic steps in the A $\beta$ 42 aggregation process consists of three stages: (i) three rounds of selection of fibril-specific scFvs from phage display libraries after removal of monomer binders (Fig. 1A and B), (ii) ranking by means of SPR assays of the fibril-binding affinity of scFvs (Fig. 1C), and (iii) kinetic screening for scFvs with the ability to cause selective suppression of fibril-catalyzed secondary nucleation (Fig. 1D). The kinetic screening relies on the fact that very different scenarios are predicted to be associated with the inhibition of primary nucleation, secondary nucleation, and elongation, respectively (Fig. 2A–C). For proof-of-principle, we used two commercially available libraries (Tomlinson I and J) (25) of scFvs displayed on protein III of the filamentous phage (26, 27).

**Monomer-binder removal and selection of fibril-specific scFvs.** Monomer-binding phages were eliminated by mixing each library with streptavidin-coated magnetic beads with biotinylated A $\beta$ 42 monomers (Fig. 1A). This step also removes phages with affinity for the beads or the test tube surfaces. The beads were removed and the supernatant added to beads coupled with biotinylated A $\beta$ 42 fibrils (Fig. 1B). After extensive washing, the members of each library with high affinity for the fibrils were eluted with acid, neutralized, and used to infect Tg1 *Escherichia coli* cells to produce enriched scFv phage display libraries. The whole procedure of monomer-binder removal and fibril-binder capture was repeated three times. The infected *E. coli* cells were then spread on LB agar plates, and 150 colonies were picked for production of single-clone phages in liquid cultures.

**Affinity ranking.** Surface plasmon resonance (SPR) technology was used for preliminary ranking of phage-scFvs in terms of their apparent affinity for A $\beta$ 42 fibrils. The 150 single-clone solutions were used to identify putative high-affinity fibril binders (Fig. 1C) by injecting them over a sensor surface with immobilized A $\beta$ 42 fibrils. Seven clones (I2, I48, I68, J44, J46, J7, and J57) were chosen for further analysis in this work and used to infect the HB2151 *E. coli* strain for expression and purification of isolated scFvs free in solution rather than displayed on phages. SPR analysis verified in each case a high affinity binding to fibrils with  $K_D$  values in the range of 0.3–2  $\mu$ M (Fig. 1D and *SI Appendix*, Fig. S1).

**Effects on microscopic steps in the A $\beta$ 42 aggregation process.** Measurements of the A $\beta$ 42 aggregation kinetics were used to analyze the effects of the scFvs on distinct microscopic steps in the fibril formation process. As an illustration of possible outcomes, we used the AmyloFit interface (28) to simulate kinetic curves resulting from the selective reduction of each of the microscopic rate constants—that is, those for primary nucleation ( $k_n$ ), secondary nucleation ( $k_2$ ), and elongation ( $k_+$ ). A reduction of  $k_n$  leads to a progressive increase in the lag time without any change

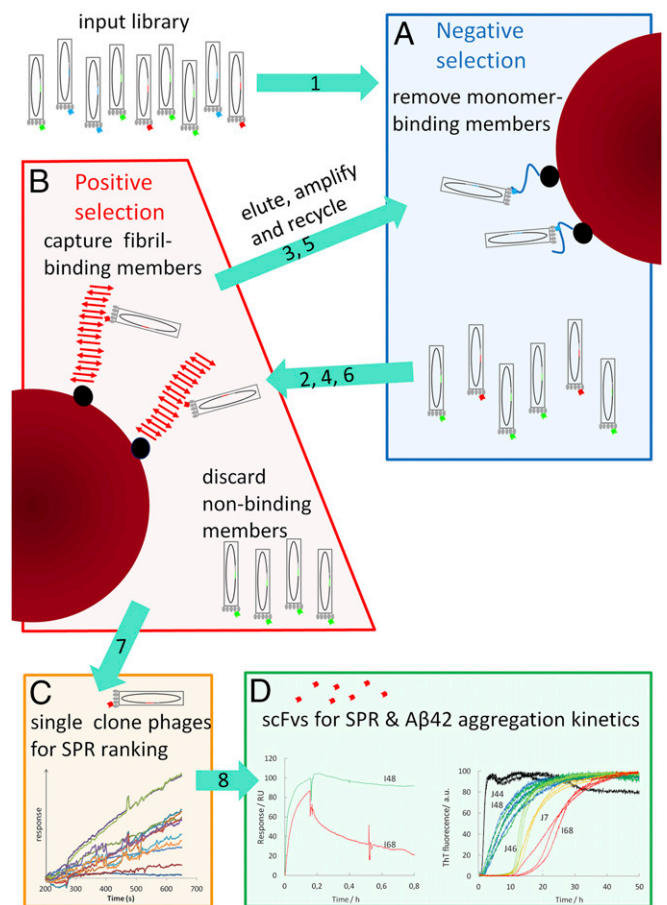


**Fig. 1.** Schematic outline of the phage display selection strategy. (Step 1) Monomer-binding members of the libraries were captured by A $\beta$ 42 monomers on magnetic beads that were removed using a magnet (negative selection, A). Ca.  $10^{13}$  virions (16 pmol) were added to 100 pmol of monomers (blue line) on beads, thus providing capacity to bind all phages displaying scFvs with high affinity for monomers. (Step 2) The solutions with unbound phages were added to magnetic beads with A $\beta$ 42 fibrils to capture phages with fibril-binding scFvs (positive selection, B), followed by extensive washing to discard nonbinding members. Fibril-bound phages were eluted with acid, neutralized, and used to infect *E. coli* to produce an enriched scFv phage display library. Step 3 = step 1, and step 4 = step 2, except that the enriched libraries from step 2 were used. Step 5 = step 1, and step 6 = step 2, except that the enriched libraries from step 4 were used. (Step 7) Fibril-bound phages were eluted with acid, neutralized, and used to infect *E. coli*, spread on LB agar plates and single clones picked for production of phages with displayed scFvs. The medium after removal of *E. coli* cells by centrifugation was used in SPR experiments for ranking their affinity for A $\beta$ 42 fibrils immobilized on sensor chips (C). (Step 8) The strongest binding candidates were used to infect *E. coli* to produce isolated scFvs for more detailed SPR analysis and A $\beta$ 42 aggregation kinetics (D).

in the steepness of the sigmoidal transition (Fig. 2A). The overall production of nuclei is effectively unchanged, although shifted to later times (Fig. 2D). By contrast, a selective reduction of  $k_2$  leads mainly to a change in the slope of the aggregation plots (Fig. 2B). It also significantly reduces the overall nucleation rate (Fig. 2E). Finally, a selective reduction of  $k_+$  leads to both an extended lag phase and a decrease in slope (Fig. 2C). The maximum rate of nucleation remains the same as absence of an inhibitor; however, the high nucleation rate persists for longer as a result of a slower depletion of free monomer through elongation (Fig. 2F). These simulations emphasize that secondary nucleation is indeed the key process that needs to be inhibited to limit the production of high levels of oligomers. To attempt to

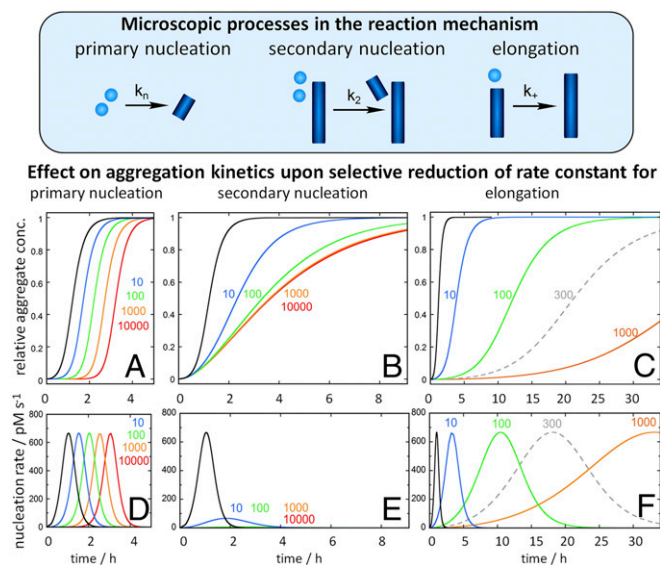


**Fig. 2.** Simulated kinetic profiles in the presence of inhibitors of discrete microscopic steps in protein aggregation reactions. (Top) Microscopic processes included in the reaction scheme. The AmyloFit interface (28) was used to simulate the changes in the time evolution of the fibril mass upon selective reduction of (A) the rate constants of primary nucleation ( $k_n$ ), (B) the rate constants of secondary nucleation ( $k_2$ ), and (C) the rate constants of elongation ( $k_+$ ). In each case, the remaining two rate constants were fixed at the values obtained for A $\beta$ 42 in 20 mM sodium phosphate buffer with 0.2 mM EDTA, pH 8.0, 37 °C. The reference (black) curves in each panel were calculated using the rate constants (20) measured for A $\beta$ 42 alone in the absence of inhibitor under the same conditions:  $k_n = 3 \times 10^{-1} \text{ M}^{-1} \text{ s}^{-1}$ ,  $k_2 = 1 \times 10^4 \text{ M}^{-1} \text{ s}^{-1}$ ,  $k_+ = 3 \times 10^6 \text{ M}^{-1} \text{ s}^{-1}$ . All calculations assumed that the reaction was initiated at time 0 from a solution containing 3  $\mu\text{M}$  A $\beta$ 42 monomer. The color codes and numbers refer to the fold-reduction of the selected microscopic rate constant (e.g., 10 indicates that the rate constant is reduced 10-fold). The rate of formation of nuclei by primary and secondary processes was calculated for the cases of selective reduction of (D)  $k_n$ , (E)  $k_2$ , and (F)  $k_+$ .

reduce the toxicity of A $\beta$ 42 through specific inhibition of secondary nucleation (Fig. 2E) (21), we set out to identify scFvs that modulate A $\beta$ 42 aggregation kinetics in a manner as close as possible to the scenario in Fig. 2B.

The intensity of ThT fluorescence as a function of time was used to monitor fibril formation for A $\beta$ 42 alone and in the presence of each of the seven scFvs (I2, I48, I68, J7, J44, J46, and J57) at concentrations ranging from 0.1 to 1.0 molar equivalents (Figs. 3A–D and 4A–C). These macroscopic aggregation curves are clearly affected by all four scFvs but not by randomly selected scFvs from the initial pool (Fig. 4D and E). The data obtained with each of the fibril-binding scFvs were fitted using the AmyloFit interface (28), with the rate constant for one microscopic process as a free parameter (different value allowed for each scFv concentration) and the other two as global parameters (same value used for all curves).

**Identification of Specific Secondary Nucleation Inhibitors.** For four of the candidate scFvs—I2, I48, J44, and J57—we found that the main effect of their presence in A $\beta$ 42 solutions was a change in the slope of the growth region (Fig. 3). The data are well fitted assuming a selective reduction of  $k_2$  (Fig. 3) but cannot be fitted at all if only  $k_n$  (SI Appendix, Fig. S2), or only  $k_+$  (SI Appendix, Fig. S3), is varied. The strongest inhibitory effect of these scFvs is thus likely to be on secondary nucleation, whereas primary nucleation and elongation remain essentially unaffected, in agreement with the scenario shown in Fig. 2B. The fits to the data at the higher scFv concentrations indicate a very low value of  $k_2$ . The effect saturates at  $\sim 1$ – $2 \mu\text{M}$  scFv in solutions containing

initially 3  $\mu\text{M}$  A $\beta$ 42 monomers, suggesting that secondary nucleation is effectively completely suppressed in the presence of high concentration of these scFvs, and the secondary nucleation rate is much lower than the primary nucleation rate essentially during the full time course of the aggregation reaction.

The plots of the secondary nucleation rate constants obtained from the fitting procedure as a function of scFv concentration (Fig. 3E and F) are qualitatively similar to binding curves, where I48, J44, and J57 appear to have high enough affinities to saturate the binding sites for the scFvs at the highest scFv concentrations used. The scFv I2 appears to have somewhat lower affinity (SI Appendix, Fig. S1), and at the highest concentrations used, its inhibitory effect corresponds to ca. 20-fold reduction in  $k_2$ , thus some secondary nucleation still occurs at a detectable

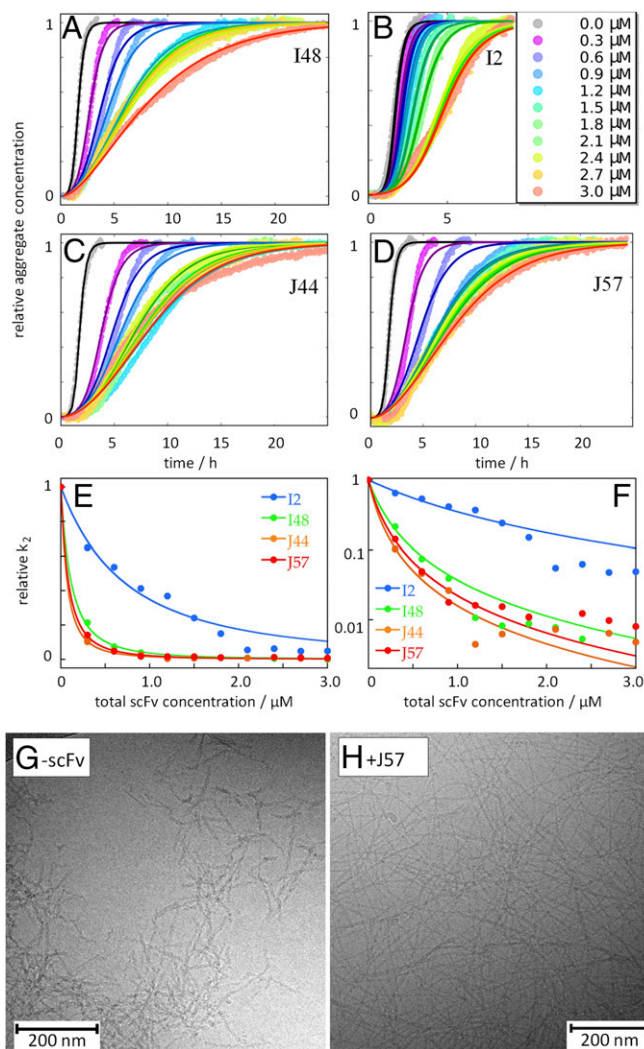


**Fig. 3.** Kinetic analyses of the effects of scFvs that were found to inhibit selectively secondary nucleation. The aggregation kinetics starting from 3  $\mu\text{M}$  A $\beta$ 42 monomer in the absence (gray) and presence of I48 (A), I2 (B), J44 (C), and J57 (D) at concentrations ranging from 0.3 to 3.0  $\mu\text{M}$  with color code shown as an Inset in B. The fitted curves shown here were generated by the AmyloFit interface (28) keeping  $k_+$  and  $k_n$  the same for all scFv concentrations, whereas the rate constant  $k_2$  was allowed to take specific values at the different scFv concentrations. (E and F) The relative change in  $k_2$  obtained from the fits in A–D, with linear and logarithmic y axis, respectively. The solid lines show fitted curves using an equation for competitive binding of the scFvs and the A $\beta$ 42 monomers for the fibril surface as described in SI Appendix. (G and H) Cryo-TEM images of A $\beta$ 42 fibrils formed in the absence (G) and presence (H) of scFv J57.

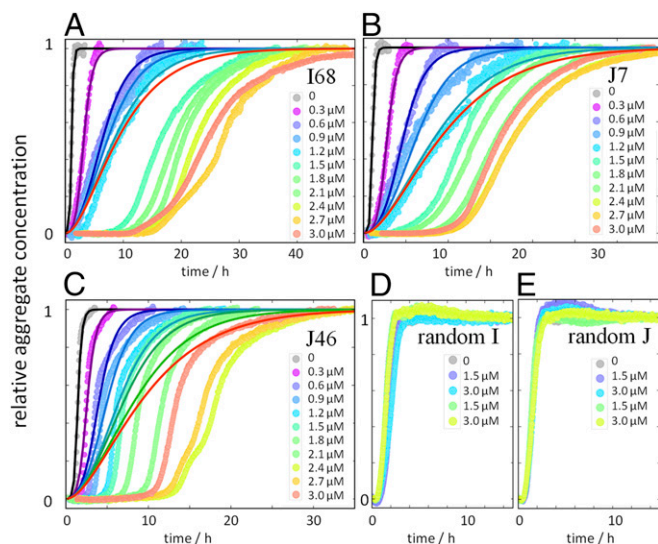


**Fig. 4.** Kinetic analyses to discard scFvs that affect other processes in addition to secondary nucleation. The aggregation kinetics of 3  $\mu\text{M}$  solutions of A $\beta$ 42 monomers in the absence (black) and presence (colors) of scFvs I68 (A), J7 (B), and J46 (C) and two control scFvs selected randomly from the I and J libraries (D and E) at 0.3–3.0  $\mu\text{M}$ . The fitted curves in A–C were generated by fixing  $k_n$  and  $k_{+}$ , allowing  $k_2$  to have different values at each scFv concentration. Note that the data for these three scFvs cannot be fitted on this assumption nor on the assumption of a selective reduction of  $k_n$ , making it likely that they also inhibit elongation.

rate. We find that the fibril-specific scFvs from clones I2, I48, J44, and J57 most likely inhibit A $\beta$ 42 aggregation through selective reduction of the rate constant for secondary nucleation. In the presence of scFvs I48, J44, and J57 at molar ratios above ca. 1:2 scFv:A $\beta$ 42, secondary nucleation has no detectable kinetic significance, although for I2 there is a residual contribution from this microscopic step.

**Morphology of the Resulting Fibrils by Cryo-EM.** The A $\beta$ 42 fibrils formed in the absence of scFv appear to have two filaments wound around each other, and there are both well-dispersed fibrils (Fig. 3G) and lumps of fibrils (SI Appendix, Fig. S4A). A $\beta$ 42 fibrils formed in the presence of scFvs J57 (Fig. 3B)—J44, I48, and I2 (SI Appendix, Fig. S4 B–D)—are overall longer, and with a reduced tendency to form larger assemblies compared with fibrils of A $\beta$ 42 alone.

**Seeded Aggregation Kinetics.** Seeded aggregation kinetics experiments were performed for A $\beta$ 42 alone and for A $\beta$ 42 in the presence of scFvs (I2, I48, J44, or J57). The monomer solution was supplemented at time 0 with preformed fibrils at a total concentration of 1%, 3%, 10%, or 30% in monomer equivalents (Fig. 5). At 1% seeds, the need for primary nucleation is bypassed and the aggregation kinetics of A $\beta$ 42 in the absence of scFv are greatly accelerated by secondary nucleation (20, 22) as shown by a decrease in the length of the lag phase (Fig. 5E). However, scFvs I2, I48, J57, and J44 diminish this seeding effect (Fig. 5 A–D) and 1% and 3% seeds have much lower catalytic effect than for A $\beta$ 42 alone. The aggregation in the presence of these scFvs is dominated by primary nucleation and still very strongly retarded relative to the behavior observed in the absence of scFv. At 30% seed, the aggregation kinetics of A $\beta$ 42 in the absence of scFv is greatly accelerated due to rapid elongation of the seeds, seen as the emergence of observable growth from time 0 (Fig. 5 E and F). The growth rate at early times can reveal effects on the elongation rate constant, and we find that I2, I48, J57, and J44 cause at most a factor of 1.3 change in this rate (Fig. 5 F and G), compared with the more than 10-fold (I2) or more than

100-fold (I48, J44, and J57) reduction in the rate constant for secondary nucleation (Figs. 3 E and F and 5G).

**Discarding ScFvs That May Inhibit Elongation.** In the presence of scFvs J7, J46, and I68, the aggregation kinetics indicate that the elongation rate constant may also be affected (Fig. 4). The curves at low concentration of scFvs J7 and I68 can be fitted if only  $k_2$  is reduced (Fig. 4 A and B). The data at a higher concentration of scFv J7 and I68 can only be fitted by assuming that  $k_{+}$  or  $k_n$  are reduced as well (SI Appendix, Fig. S5), suggesting that elongation may be affected. J46 appears to affect the elongation rate at all concentrations (Fig. 4C). As a result of these findings, none of these three scFvs are considered further for further studies.

**The Amino Acid Sequences of the Selected ScFvs.** DNA sequencing was used to elucidate the amino acid sequences of the scFvs that selectively inhibit secondary nucleation (I2, I48, J44, and J57; SI Appendix, Table S2). The amino acid compositions in the variable positions of the complementarity-determining regions (CDRs) of these scFvs were compared with the respective libraries from which they originate (Fig. 6). Although the sample size is small, for the clones from the Tomlinson I library, we find an enrichment of N and T residues. For the selected Tomlinson J clones, we find an enrichment of N, T, R, K, Y, and A, whereas the largest hydrophobic residues in this library (F, L, I, M, and W) are totally absent. The enrichment of R and K can be rationalized on the basis of the net negative charge of A $\beta$ 42 fibrils. Positively charged or large hydrophobic residues are not present in the I library. Cysteine is present in both libraries but is not found in any of the selected clones, meaning that none of the observed effects are due to aberrant disulfide-bond formation.

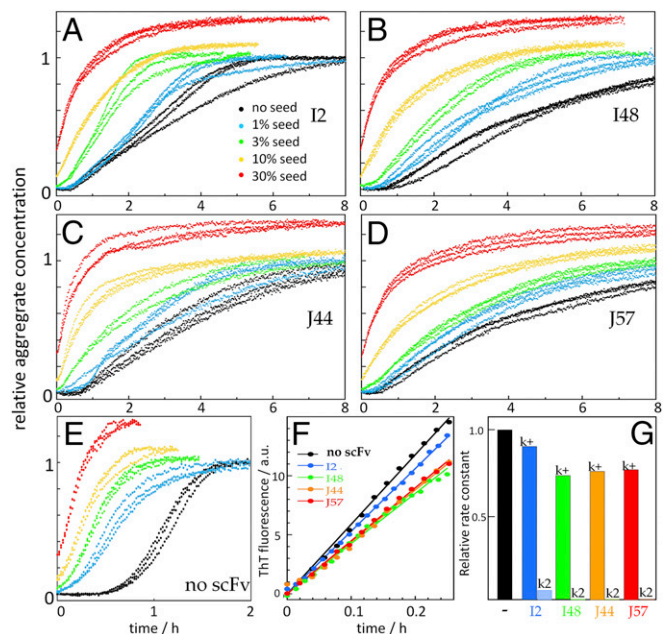


**Fig. 5.** Seeded aggregation kinetics. Shown are the aggregation kinetics of solutions of 3  $\mu\text{M}$  A $\beta$ 42 monomer in the absence (E) or presence of 2  $\mu\text{M}$  scFv I2 (A), I48 (B), J44 (C), and J57 (D) supplemented with no (black), 30 nM (cyan), 90 nM (green), 300 nM (yellow), or 900 nM (red) seeds at time 0. The initial slopes in the presence of 30% (900 nM) seed fibrils (F) were fitted using straight lines. (G) The obtained elongation rate constant,  $k_{+}$ , relative to the case of no seed is shown as bars, and the rate constant for secondary nucleation,  $k_2$ , relative to the case of no seed is shown as bars in lighter colors.

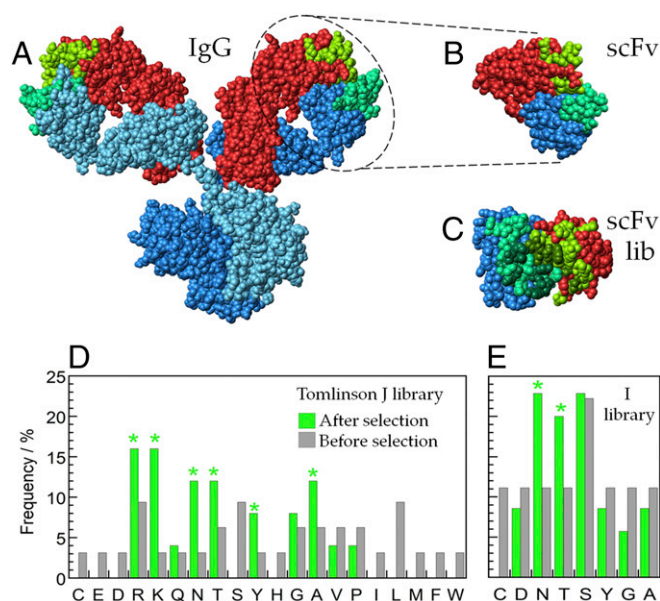


**Fig. 6.** The scFv structure and amino acid compositions. (A) Space-filling model of an IgG (molecular mass, 150 kDa; PDB ID code 1IGY) with the two heavy chains in blue, the two light chains in red, and the residues in the CDR regions in green. (B and C) An scFv (molecular mass, 27 kDa; PDB ID code 5DFW) including the variable domain of one heavy chain ( $V_H$ ) and one light chain ( $V_L$ ). In C, the scFv is rotated to get a better view of the CDRs, and the 18 residues that are varied in CDR2 and CDR3 of  $V_H$  and  $V_L$  in the Tomlinson libraries are shown in darker green. (D and E) Result of DNA sequencing of the four scFvs that inhibit secondary nucleation (I2, I48, J44, and J57). For each library (I and J), the observed average frequency of each amino acid in the 18 diversified positions in the selected clones (green bars) is compared with the average frequency in the libraries (gray bars). Green asterisks indicate enrichment after selection.

## Discussion

We discuss in this paper a strategy to derive scFvs that specifically bind amyloid fibrils and inhibit fibril-dependent microscopic processes. This strategy relies on the detailed mechanistic understanding of the aggregation process of A $\beta$ 42 associated with the onset and development of AD (20). Previous studies have identified a series of microscopic steps in the process of aggregation that together contribute to the overall macroscopic kinetic profile of the reaction and have revealed the importance of the catalytic conversion of monomeric species into aggregates as a result of secondary nucleation on fibril surfaces. This process results in the production of neurotoxic oligomeric species (20, 21) with distinct intracellular targets (29).

Previous studies have shown that molecular chaperones (21, 30), metal ions (31), and small molecules (32, 33) may inhibit one or more of the underlying microscopic steps in the overall A $\beta$ 42 aggregation process, and the selective inhibition of secondary nucleation has been observed with both proteins and small molecules. At the molecular level, a given inhibitor may interact particularly favorably with one of the species present during the aggregation reaction (34). Some inhibitors suppress a single microscopic step, whereas others act on more than one step, depending on whether the inhibitor interacts with monomers, oligomers, or fibrils (23, 24, 34). If this species is the monomer, the primary and secondary nucleation and elongation events will all be affected, albeit to different degrees. If the inhibitor interacts with one of the aggregated species, by contrast, the effect will be more specific. In particular, if binding occurs specifically to the fibrils, either elongation or secondary nucleation, or both, may be inhibited.

The search for secondary nucleation inhibitors was motivated by their ability to reduce dramatically the number of A $\beta$ 42 oligomers

produced in their presence (Fig. 2E) (21) and their ability to reduce A $\beta$ 42 toxicity as demonstrated through electrophysiology measurements of  $\gamma$ -oscillations in brain slices (21). By contrast, suppression of elongation does not alter the maximum rate of oligomer generation and indeed could lead to an increase in toxicity because oligomer generation can maintain significant levels during a longer time frame when monomer consumption through elongation is inhibited. The total number of oligomers generated due to secondary (and primary) nucleation may increase several-fold if elongation is inhibited because fewer monomers are consumed in the elongation process (Fig. 2F).

Our search for secondary nucleation inhibitors is facilitated by their distinct macroscopic signature of a reduced slope of the growth phase of the aggregation reaction (Fig. 2B) and from the saturation of the observed effects at high inhibitor concentrations when the scFvs cover all of the catalytic sites on the fibril surface (21). Moreover, we exploit the fact that very different scenarios can be expected upon inhibition of primary nucleation or elongation (Fig. 2A and C). The identification of scFvs I2, I48, J44, and J57 as secondary nucleation inhibitors relies on the much-enhanced fits to the data of the integrated rate laws when rate constants for secondary (Fig. 3) rather than primary nucleation or elongation (*SI Appendix*, Figs. S2 and S3) are varied and the direct confirmation of these findings through analysis of seeded aggregation reactions (Fig. 5).

As a consequence of secondary nucleation inhibition, the reactive flux is redirected to a pathway including primary nucleation and elongation only. This means that a much smaller number of new aggregates are created (Fig. 2E) and a larger fraction of monomers are consumed in elongation of those fewer aggregates, leading to longer fibrils on average. Although length estimates from cryo-EM images are likely biased by the greater ease of looking at dispersed fibrils, it is obvious that many of the fibrils formed in the presence of scFvs span the entire field of view (Fig. 3H and *SI Appendix*, Fig. S4 B–D), meaning they are over 1  $\mu$ m long, whereas many of the fibrils formed in the absence of scFvs are around 200–500 nm long (Fig. 3G and *SI Appendix*, Fig. S4A). Another interesting feature of fibrils formed in the presence of scFv is their apparent lower tendency toward higher order assembly in lumps. This suggests that their surface properties are altered due to binding of scFvs to the fibrils.

**Monovalent ScFvs May Be Selected as Fibril-Specific.** The use of scFvs, which have a single epitope-binding site (Fig. 6), and removal of monomer binders (Fig. 1) are important features of our methodology; this enables targeting of epitopes present in fibrils but not in monomers. The single binding site avoids the generation of fibril specificity as a result of the chelate effect (avidity), which was recently found to explain the apparent fibril specificity of intact antibodies that recognize with low affinity an epitope found in the monomer; each IgG molecule may bind simultaneously to two epitopes in species consisting of more than one monomer (35). An scFv can only be fibril-specific if it binds to an epitope that is present in fibrils but not in monomers and can therefore not be mimicked by short fragments of the A $\beta$ 42 peptide (*SI Appendix*, Figs. S6 and S7). In addition to the relatively disordered N terminus (residues 1–15), side chains of K16, V18, A21, E22, D23, S26, K28, V40, and A42 are exposed on the surface of A $\beta$ 42 fibrils (11, 12). Fibril-specific epitopes might include several of these residues, or features containing copies of the same amino acid in multiple fibril planes (11). The apparent enrichment of uncharged hydrophilic residues—N, T, and Y (Fig. 6)—suggests that hydrogen bonding features may be important determinants of the fibril specificity.

**Secondary Nucleation and Elongation Occur at Separate Sites.** The discovery of a group of scFvs that selectively inhibits secondary nucleation, and another that also inhibits elongation, implies that

distinct 3D epitopes are likely to exist along the lengths and at the ends of fibrils and that separate features of the fibril are involved in elongation and in secondary nucleation. Indeed, if the sites for secondary nucleation and elongation were to be identical, it would not be possible to block selectively secondary nucleation without affecting elongation and vice versa. The scFvs I2, I48, J44, and J57 act in a manner similar to Brichos, which binds along the fibril surface (21) and blocks selectively secondary nucleation. These scFvs are likely to bind to epitopes presented along the sides of the fibrils in a manner that prevents A $\beta$ 42 monomer binding or nucleation. The scFvs I68 and J7 are intriguing in that they seem to show a duality of behaviors, with selective inhibition of secondary nucleation processes at low concentration, whereas at higher concentrations the elongation step also appears to be affected (Fig. 4 *A* and *B* and *SI Appendix*, Fig. S5). These scFvs are likely to have affinity for epitopes both along the fibrils and at the fibril ends, where scFv binding will inhibit elongation.

**Potential Significance of the Present Findings.** A large number of studies have reported that oligomeric species, formed during the process of aggregation, are the most highly cytotoxic species associated with protein misfolding (14, 15, 36). Secondary nucleation is a positive feedback mechanism that can lead to the rapid amplification of the number of aggregates once an initial population has been formed (20, 22) and also be very effective in the production of toxic oligomers (20, 21). Inhibition of secondary nucleation, therefore, appears likely to be an important approach to reduce the pathogenicity associated with protein aggregation (34). Indeed, the discovery that specific molecular chaperones can act in a highly selective manner to suppress secondary nucleation suggests that this approach is exploited by living systems to reduce the risks of protein aggregation *in vivo*. Selection of fibril-binding antibodies from phage display libraries is therefore a fruitful route toward identifying inhibitors with the potential both to act as therapeutics and to increase our

understanding of the mechanism of protein aggregation and also to elucidate further the origins and means of progression of some of the most highly debilitating of all human diseases.

## Conclusions

We have shown in this study that screening of phage display libraries for antibody fragments (scFvs) that bind to amyloid fibrils, combined with affinity ranking and kinetic screening, enables the identification of antibodies with the capacity to inhibit fibril-dependent secondary nucleation processes. Importantly, our approach allows scFvs that inhibit elongation to be detected and eliminated from further investigations, as such species can cause significant apparent inhibition of the overall aggregation reaction but are unlikely to result in a significant reduction of toxic species and could even lead to an increase in the overall production of oligomers. The results suggest further that scFvs generated from such a systematic approach are likely to be favorable starting points for the development of future therapeutic strategies designed to combat AD. In addition, the approach described in this study of A $\beta$ 42 should be generally applicable to other pathogenic amyloid proteins for which secondary nucleation leads to autocatalytic amplification and the rapid proliferation of toxic oligomers and may represent a general strategy to find potential therapeutic agents directed at the wider range of protein misfolding diseases.

## Materials and Methods

A $\beta$ 42 purification, monomer isolation, bead-conjugation, phage display studies, scFv production and purification, SPR experiments, aggregation kinetics measurements and analysis, and cryo-EM were performed essentially as described (20, 21, 25, 37). See *SI Appendix*, *Materials and Methods*.

**ACKNOWLEDGMENTS.** This work was funded by the European Research Council (S.L.); the Swedish Research Council (VR) (S.L. and J.P.); Sidney Sussex College, Cambridge (G.M.); the Wellcome (C.M.D., M.V., and T.P.J.K.) and Leverhulme Trusts (C.M.D.); and the Frances and Augustus Newman Foundation (T.P.J.K.).

- Chiti F, Dobson CM (2006) Protein misfolding, functional amyloid, and human disease. *Annu Rev Biochem* 75:333–366.
- Knowles TP, Vendruscolo M, Dobson CM (2014) The amyloid state and its association with protein misfolding diseases. *Nat Rev Mol Cell Biol* 15:384–396.
- Hebert LE, Weuve J, Scherr PA, Evans DA (2013) Alzheimer disease in the United States (2010–2050) estimated using the 2010 census. *Neurology* 80:1778–1783.
- Selkoe DJ (2013) The therapeutics of Alzheimer's disease: Where we stand and where we are heading. *Ann Neurol* 74:328–336.
- Hardy J, Allsop D (1991) Amyloid deposition as the central event in the aetiology of Alzheimer's disease. *Trends Pharmacol Sci* 12:383–388.
- Head E, Lott IT (2004) Down syndrome and beta-amyloid deposition. *Curr Opin Neurol* 17:95–100.
- Blennow K, de Leon MJ, Zetterberg H (2006) Alzheimer's disease. *Lancet* 368:387–403.
- Haass C, Selkoe DJ (2007) Soluble protein oligomers in neurodegeneration: Lessons from the Alzheimer's amyloid  $\beta$ -peptide. *Nat Rev Mol Cell Biol* 8:101–112.
- Lendel C, et al. (2014) A hexameric peptide barrel as building block of amyloid- $\beta$  protofibrils. *Angew Chem Int Ed Engl* 53:12756–12760.
- Astbury WT, Dickinson S, Bailey K (1935) The X-ray interpretation of denaturation and the structure of the seed globulins. *Biochem J* 29:2351–2360.1.
- Colvin MT, et al. (2016) Atomic resolution structure of monomorphic A $\beta$ 42 amyloid fibrils. *J Am Chem Soc* 138:9663–9674.
- Wälti MA, et al. (2016) Atomic-resolution structure of a disease-relevant A $\beta$ (1–42) amyloid fibril. *Proc Natl Acad Sci USA* 113:E4976–E4984.
- Parthasarathy S, et al. (2015) Structural insight into an Alzheimer's brain-derived spherical assembly of amyloid  $\beta$  by solid-state NMR. *J Am Chem Soc* 137:6480–6483.
- Walsh DM, et al. (2002) Naturally secreted oligomers of amyloid beta protein potentially inhibit hippocampal long-term potentiation *in vivo*. *Nature* 416:535–539.
- Jan A, et al. (2011) Abeta42 neurotoxicity is mediated by ongoing nucleated polymerization process rather than by discrete Abeta42 species. *J Biol Chem* 286:8585–8596.
- Gandy S, DeKosky ST (2013) Toward the treatment and prevention of Alzheimer's disease: Rational strategies and recent progress. *Annu Rev Med* 64:367–383.
- Marciani DJ (2016) A retrospective analysis of the Alzheimer's disease vaccine progress - The critical need for new development strategies. *J Neurochem* 137:687–700.
- Roher AE, et al. (2013) Bapineuzumab alters a $\beta$  composition: Implications for the amyloid cascade hypothesis and anti-amyloid immunotherapy. *PLoS One* 8:e59735.
- Sevigny J, et al. (2016) The antibody aducanumab reduces A $\beta$  plaques in Alzheimer's disease. *Nature* 537:50–56.
- Cohen SI, et al. (2013) Proliferation of amyloid- $\beta$ 42 aggregates occurs through a secondary nucleation mechanism. *Proc Natl Acad Sci USA* 110:9758–9763.
- Cohen SIA, et al. (2015) A molecular chaperone breaks the catalytic cycle that generates toxic A $\beta$  oligomers. *Nat Struct Mol Biol* 22:207–213.
- Arosio P, Cukalevski R, Frohm B, Knowles TP, Linse S (2014) Quantification of the concentration of A $\beta$ 42 propagons during the lag phase by an amyloid chain reaction assay. *J Am Chem Soc* 136:219–225.
- Arosio P, Vendruscolo M, Dobson CM, Knowles TP (2014) Chemical kinetics for drug discovery to combat protein aggregation diseases. *Trends Pharmacol Sci* 35:127–135.
- Arosio P, et al. (2016) Kinetic analysis reveals the diversity of microscopic mechanisms through which molecular chaperones suppress amyloid formation. *Nat Commun* 7:10948.
- de Wildt RM, Mundy CR, Gorick BD, Tomlinson IM (2000) Antibody arrays for high-throughput screening of antibody-antigen interactions. *Nat Biotechnol* 18:989–994.
- Smith GP (1985) Filamentous fusion phage: Novel expression vectors that display cloned antigens on the virion surface. *Science* 228:1315–1317.
- McCafferty J, Griffiths AD, Winter G, Chiswell DJ (1990) Phage antibodies: Filamentous phage displaying antibody variable domains. *Nature* 348:552–554.
- Meisl G, et al. (2016) Molecular mechanisms of protein aggregation from global fitting of kinetic models. *Nat Protoc* 11:252–272.
- Dunning CJ, et al. (2016) Direct high affinity interaction between A $\beta$ 42 and GSK3 $\alpha$  stimulates hyperphosphorylation of Tau. A new molecular link in Alzheimer's disease? *ACS Chem Neurosci* 7:161–170.
- Månsson C, et al. (2014) Interaction of the molecular chaperone DNAJB6 with growing amyloid-beta 42 (A $\beta$ 42) aggregates leads to sub-stoichiometric inhibition of amyloid formation. *J Biol Chem* 289:31066–31076.
- Abelein A, Gräslund A, Danielsson J (2015) Zinc as chaperone-mimicking agent for retardation of amyloid  $\beta$  peptide fibril formation. *Proc Natl Acad Sci USA* 112:5407–5412.
- Habchi J, et al. (2016) An anticancer drug suppresses the primary nucleation reaction that initiates the production of the toxic A $\beta$ 42 aggregates linked with Alzheimer's disease. *Sci Adv* 2:e1501244.
- Habchi J, et al. (2017) Systematic development of small molecules to inhibit specific microscopic steps of A $\beta$ 42 aggregation in Alzheimer's disease. *Proc Natl Acad Sci USA* 114:E200–E208.
- Arosio P, Meisl G, Andreassen M, Knowles TP (2015) Preventing peptide and protein misbehavior. *Proc Natl Acad Sci USA* 112:5267–5268.
- Brännström K, et al. (2014) A generic method for design of oligomer-specific antibodies. *PLoS One* 9:e90857.
- Bucciantini M, et al. (2002) Inherent toxicity of aggregates implies a common mechanism for protein misfolding diseases. *Nature* 416:507–511.
- Walsh DM, et al. (2009) A facile method for expression and purification of the Alzheimer's disease-associated amyloid beta-peptide. *FEBS J* 276:1266–1281.

## Phage display and kinetic selection of antibodies that specifically inhibit amyloid self-replication - Supplementary material

Anna Munke, Jonas Persson, Tanja Weiffert, Erwin De Genst, Georg Meisl, Paolo Arosio, Anna Carnerup, Christopher M Dobson, Michele Vendruscolo, Tuomas PJ Knowles, Sara Linse

### Materials and Methods

*Aβ42 preparation and bead-conjugation.* The amyloid β peptide Aβ(M1-42), here referred to as Aβ42, with the amino acid sequence MDEAFRHDSGYEVHHQKLVFFAEDVGSNKGAIIGLMVGGVVIA was expressed in *Escherichia coli* and purified as described previously.<sup>37</sup> The starting ATG codon gives the sequence an N-terminal methionine that does not affect its properties significantly relative to the wild type sequence as discussed previously.<sup>37</sup> The monomeric form was isolated by dissolving lyophilized Aβ42 in 1 mL 6 M GuHCl and subjected to size exclusion chromatography on a Superdex 75 10/300 column in 20 mM sodium phosphate buffer pH 8.0, 200 μM EDTA and 0.02% sodium azide (buffer A). The fraction corresponding to the monomer was collected on ice in a low-binding tube (Genuine Axygen Quality, Microtubes, MCT-200-L-C, Union City, CA) and the concentration was determined by absorbance at 280 nm using  $\epsilon_{280} = 1440 \text{ M}^{-1}\text{cm}^{-1}$ . Fibrils of Aβ42 were generated in 96-well half-area, PEG coated polystyrene plates (Corning 3881) at 37°C. To ensure only the fibrillar aggregates were collected, 6 μM thioflavin T (ThT, Calbiochem, San Diego, CA) was added to the solution and fibril formation was followed by measuring the ThT fluorescence in a plate reader (Fluostar Optima or Fluostar Omega, BMG Labtech, Offenburg, Germany) with the excitation and emission at 440 and 480 nm, respectively. Monomer and fibrils were biotinylated separately using amine reactive reagent (NHS-sulfo-link-biotin, Thermo Fischer, Waltham, MA) followed by removal of excess reagent using gel filtration (monomer) or centrifugal filter (fibril). Biotinylated Aβ42 monomers and fibrils were separately immobilized on streptavidin-coated beads (Dynabeads M-280, Dynal, Oslo) by mixing 50 μg peptide with 1 mg beads in buffer A. The suspensions were incubated for one hour after which 10 μl 10 mM biotin was added followed by extensive washing with buffer A. All procedures involving the monomer were performed on ice to reduce the extent of aggregation.

*Phage display studies.* The Tomlinson libraries I and J (for composition see [Table S3](#)) were obtained from The Medical Research Council (MRC), Cambridge, England, and used in the selection of fibril specific scFvs following the standard protocol recommended for amplifying and using the libraries as specified in the manual provided together with the libraries (<http://docplayer.net/30268507-Human-single-fold-scfv-libraries-i-j-tomlinson-i-j.html> - accession date 25 May 2017). Every round of selection was initiated by a negative selection procedure to deplete the libraries of monomer-binding scFvs. To achieve this objective, each library (I or J, or amplified I or J library after the previous selection round) was incubated with streptavidin-coated magnetic beads treated with biotinylated Aβ42 monomer for 30 min. The beads with captured monomer-binding phages were then collected at the wall of each

tube using a magnet. The supernatants were then added to the beads coated with biotinylated A $\beta$ 42 fibrils and incubated for 60-120 min. The beads were again collected at the tube wall using a magnet, the solution removed followed by extensive washing (ten times), involving repeated dispersion and collection at the tube wall and exchange of PBS (10 mM sodium phosphate buffer with 137 mM NaCl, 3.7 mM KCl) with 0.1% Tween-20.

The fibril-bound phages were eluted with acid, neutralized by adding Tris from a concentrated stock and then used to infect *E. coli*. The phages with displayed scFvs have a non-functional protein III, therefore helper phage with functional protein III was added during the infection step, according to the Tomlinson manual. The infected *E. coli* cells were grown in liquid culture to produce enriched scFv phage display libraries, according to the Tomlinson manual, while a small amount was set aside from each sample for plating on LB agar plates to enable quantification of the yield. The enriched scFv phage display libraries were then used in a new round of selection, and the whole procedure of monomer-binder removal and fibril-binder selection was repeated three times. The total amount of the bead-conjugated monomers used during negative selection was 100 pmol in all three rounds. The total concentration of bead-conjugated fibrils during selections may be lower as the beads do not capture as much fibrils for steric reasons. After the third round of selection, 150 single colonies were picked from the LB agar plates for the production of single-clone phages in liquid cultures (2 mL LB per colony).

*scFv production and purification.* To produce soluble scFvs free from phages, the *E. coli* strain HB2151 was infected with selected phage clones in accordance with the Tomlinson manual. In contrast to the amber suppressor strain used for phage propagation (TG-1), the HB2151 *E. coli* strain does not produce phages but rather each scFv is produced and transported to the periplasmic space in soluble form due to the pelB leader sequence. Stock cultures of the transfected *E. coli* strain HB2151 in 20% glycerol were used to generate pre-cultures of the selected scFvs over-night in 50 mL Luria-Bertani (LB) medium containing 50  $\mu$ g/ml ampicillin (Duchela Biochemie, Haarlem, The Netherlands). 2.5 ml of each pre-culture was used to inoculate 500 ml LB medium with 50  $\mu$ g/ml ampicillin. The cultures were grown at 37°C and 125 rpm until OD<sub>600</sub> reached ca. 1, followed by induction with 2 mM isopropyl  $\beta$ -D-1-thiogalactopyranoside (IPTG). Expression was carried out for 20 h at 30°C with constant shaking (125 rpm) before harvesting the cells by centrifugation at 8983g for 20 min. The periplasmic protein fractions were prepared by re-suspending the bacterial pellet in 12.5 ml ice cold periplasmic extraction buffer (30 mM Tris-HCl, pH 8.0, 20% sucrose, 1 mM EDTA), and centrifuged at 17500 x g for 20 min. To prepare an osmotic shock fraction, the pellet was resuspended in 12.5 ml ice-cold osmotic shock buffer (5 mM MgSO<sub>4</sub>) and centrifuged at 17500 x g for 20 min. Before both centrifugation steps, the buffer-cell suspensions were incubated on ice for 20 min. The fractions were concentrated using a 10 kDa MWCO Vivaspin (Sartorius, Goettingen, Germany) and centrifuged at 10000 x g at 4°C. The periplasmic supernatant was concentrated down to  $\leq$  2.5 ml before the osmotic supernatant was added and the solution was again concentrated, this time to  $\leq$  2 ml. Tris-HCl (20 mM, pH 8.0) was added to the Vivaspin unit to give a total volume of 20 ml and the solution was again concentrated to  $<$  2 ml. Anion exchange purification of the scFv concentrate was carried out

either stepwise in tubes or using an anion exchange column; 500  $\mu$ l (dry volume) Sephacel DEAE (GE Healthcare, Uppsala, Sweden) per 500 ml culture was used for the purification in tubes. The scFv concentrate was incubated with Sephacel on a rocking table with 20 mM Tris-HCl pH 8.0 to a total volume of 10 ml at 4°C for 30 min. Three washing steps with the same Tris buffer were carried out, and stepwise elution was performed by adding two bed volumes of Tris buffer with increasing NaCl concentration (50 mM, 100 mM, 150 mM, 200 mM, and 300 mM to 1000 mM). After each addition the tube was inverted 60 times and centrifuged at 6150 x g for 1 min. Purification by anion exchange chromatography (HiTrap DEAE FF, 5 mL, GE Healthcare) was performed with 20 mM Tris-HCl, pH 7.6 and the samples were eluted by a 0-600 mM NaCl gradient. The next purification step was size exclusion chromatography in 20 mM sodium phosphate pH 8.0, 200  $\mu$ M EDTA, 0.02% NaN<sub>3</sub> using a Superdex 200 (GE Healthcare) column (SEC) and a fast liquid protein chromatography (FPLC) system (BioLogic DuoFlow from BioRad, Hercules, CA). Fractions were collected every minute based on the absorbance at 280 nm, and analysed on a 15% SDS-PAGE gel. Pure fractions containing the scFvs were then concentrated using a 10 kDa MWCO Vivaspin filter. Seven scFvs were successfully expressed and purified. For J44, I48, J46, J7, J57 and I68, the yield was 1-6 mg per litre cell culture at a purity of 70-90%; I2 showed lower level periplasmic expression, ca 0.5 mg/L. To avoid domain swapped scFv dimers, the monomer fraction was isolated by gel filtration just prior to the kinetic experiments.

*Surface plasmon resonance experiments.* All SPR experiments were performed using a BIAcore 3000 system (BIAcore AB, Uppsala, Sweden). A $\beta$ 42 fibrils were immobilized on CM5 sensorchip surfaces “offline”, i.e. not in the machine. The sensorchip surfaces were activated by adding 50  $\mu$ l a mixture of EDC and NHS and incubating for 30 min at room temperature. This step was repeated with fresh solution after which the chip was washed three times with PBS. A solution of A $\beta$ 42 fibrils (50  $\mu$ l of a 12  $\mu$ g/ml fibrils in 10 mM NaAc pH 4.5) was then added to the chip, which was incubated overnight at room temperature. The surface was washed five times with PBS followed by inactivation with ethanolamine. The chip was then docked in the machine and the surface was inactivated twice more before use in the kinetics experiment with phage-scFv or purified scFv solutions.

After the screening of the phage display libraries for fibril-specific scFvs, we performed a preliminary affinity ranking of phage-displayed scFvs using SPR. While phage-ELISA is a common method for affinity ranking,<sup>38</sup> studies have shown that SPR can be used to select high affinity binders among phage-displayed proteins.<sup>39</sup> The successful identification of isolated scFvs from all 7 selected clones as inhibitors of fibril-dependent processes, and of 4 out of 7 as specific inhibitors of secondary nucleation, validates our approach of using SPR to identify a reasonable number of phage-displayed scFv clones for production and purification of isolated scFvs for the subsequent detailed kinetic and binding analyses.

*Aggregation kinetics by ThT fluorescence.* The kinetic experiments were performed essentially as described,<sup>40</sup> but with no shaking between measurements, and data were read every 60 s. A dilution series of 11 samples with concentrations ranging from 0 to 3  $\mu$ M was

prepared for each scFv in low binding Eppendorf tubes (Genuine Axygen Quality, Microtubes, MCT-200-L-C) with 3  $\mu\text{M}$  A $\beta$ 42 and 6  $\mu\text{M}$  ThT and kept on ice before starting the experiments. Triplicates of each sample were loaded into a 96-well half-area plate of black polystyrene with a clear bottom and PEG coating (Corning 3881) and sealed with a plastic film (Corning 3095 or SealPlate Sigma Aldrich). Fibril formation was followed at 37°C by measuring the ThT fluorescence every 1 or 3 min using an Omega or Galaxy Fluostar plate reader (BMG Labtech, Offenburg, Germany). The excitation and emission wavelengths were set at 440 and 480 nm, respectively. As a control, a sample of scFv without A $\beta$ 42 was incubated with ThT, and no increase in ThT fluorescence signal was observed.

*Kinetic analysis of the microscopic mechanisms of inhibition of scFvs.* We performed a kinetic analysis to determine which microscopic processes were affected by the presence of the different scFvs. To this effect, the kinetic data acquired at a reference A $\beta$ 42 concentration in the absence and presence of different concentrations of scFvs were analysed based on the integrated rate law for the aggregation of A $\beta$ 42,<sup>20</sup> and the calculated profiles were fitted to the experimental data using the AmyloFit platform.<sup>28</sup> As in previous work,<sup>21</sup> the depolymerisation rate was assumed to be a negligible contribution to the overall kinetics based on the very low backward rates compared to the time-scale of aggregation. The assumption of negligible depolymerisation rate was verified in our previous work on the aggregation of A $\beta$ 42.<sup>20</sup> In order to analyse the effect of scFvs on the individual microscopic processes we used the same set of kinetic parameters in the fit for different concentrations of scFv with the exception of the rate constant corresponding to the microscopic process that was tested. The rate constants that are antibody-independent are defined as the “global fit” (i.e. enforced to have a single value at all scFv concentrations) while the variable rate constant is set to “fit” (i.e. allowed to have a different value at each scFv concentration). The values of the variable rate constants obtained by the individual fits to single kinetic profiles were recorded. This process was repeated by considering different variable rate constants: the rate constants of primary nucleation,  $k_n$ , secondary nucleation,  $k_2$ , and elongation,  $k_+$ . For details see steps 42 to 49 in the protocol of Meisl et al.<sup>28</sup>

*A note on combined rate constants:* For unseeded data, only the products of the rate constants, namely  $k_+k_n$  and  $k_+k_2$ , are constrained, but not the individual rate constants. However, we can still selectively investigate a variation of  $k_+$ ,  $k_n$  and  $k_2$ ; for example, a variation of  $k_n$  would appear as a variation of  $k_+k_n$  and an unchanged  $k_+k_2$ . This same effect could in theory also be observed if  $k_+$  and  $k_n$  change in a completely correlated manner, i.e. one rate decreases by the same factor the other increases; however, such a case is sufficiently unlikely to be neglected here. In addition, we provide seeded experiments that avoid the issues arising from an inability to determine the individual rates separately.

*Cryo-EM.* Samples of 6  $\mu\text{M}$  A $\beta$ 42 monomer with and without 6  $\mu\text{M}$  scFv were incubated at 37°C in PEGylated plates (Corning 3881) in a plate reader and collected after reaching the plateau in ThT fluorescence. Specimens for electron microscopy were prepared in a controlled environment vitrification system (CEVS) to ensure stable temperature and to avoid loss of solution during sample preparation. The specimens were prepared as thin liquid films, <300

nm thick, on lacey carbon filmed copper grids and plunged into liquid ethane at  $-180^{\circ}\text{C}$ . This leads to vitrified specimens, avoiding component segmentation and rearrangement, and the formation of water crystals, thereby preserving original microstructures. The vitrified specimens were stored under liquid nitrogen until measured. A Fischione Model 2550 cryo transfer tomography holder was used to transfer the specimen into the electron microscope, JEM 2200FS, equipped with an in-column energy filter (Omega filter), which allows zero-loss imaging. The acceleration voltage was 200kV and zero-loss images were recorded digitally with a TVIPS F416 camera using SerialEM under low dose conditions with a 30 eV energy selecting slit in place.

## Supplementary results

### SPR analysis of scFv binding to immobilized A $\beta$ 42 fibrils.

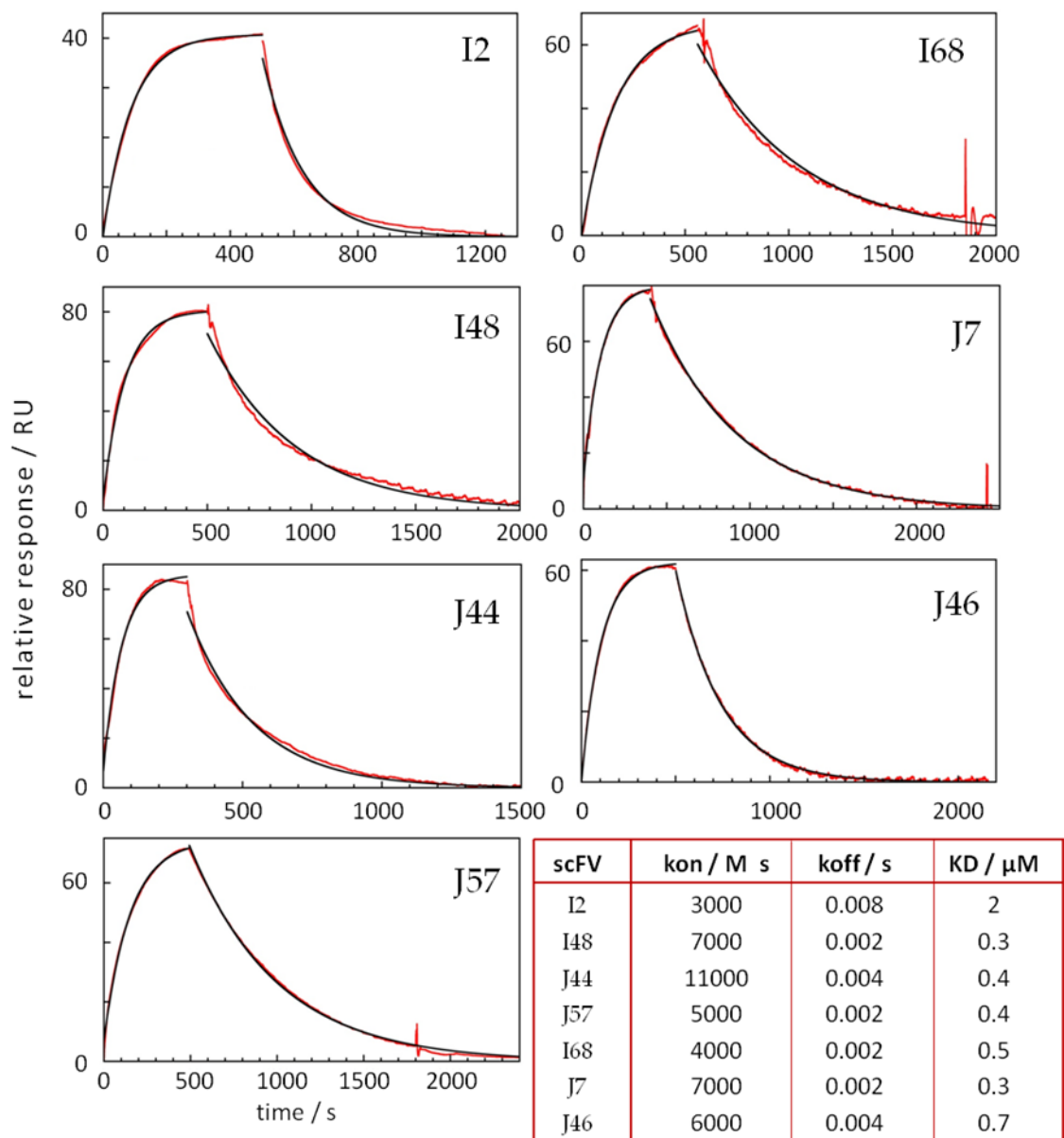


**Figure S1.** SPR data. Seven scFvs were injected one-by-one at three different concentrations (0.25, 0.5 and 1  $\mu M$ ) over a CM3 sensorchip with immobilized A $\beta$ 42 fibrils, followed by buffer flow.

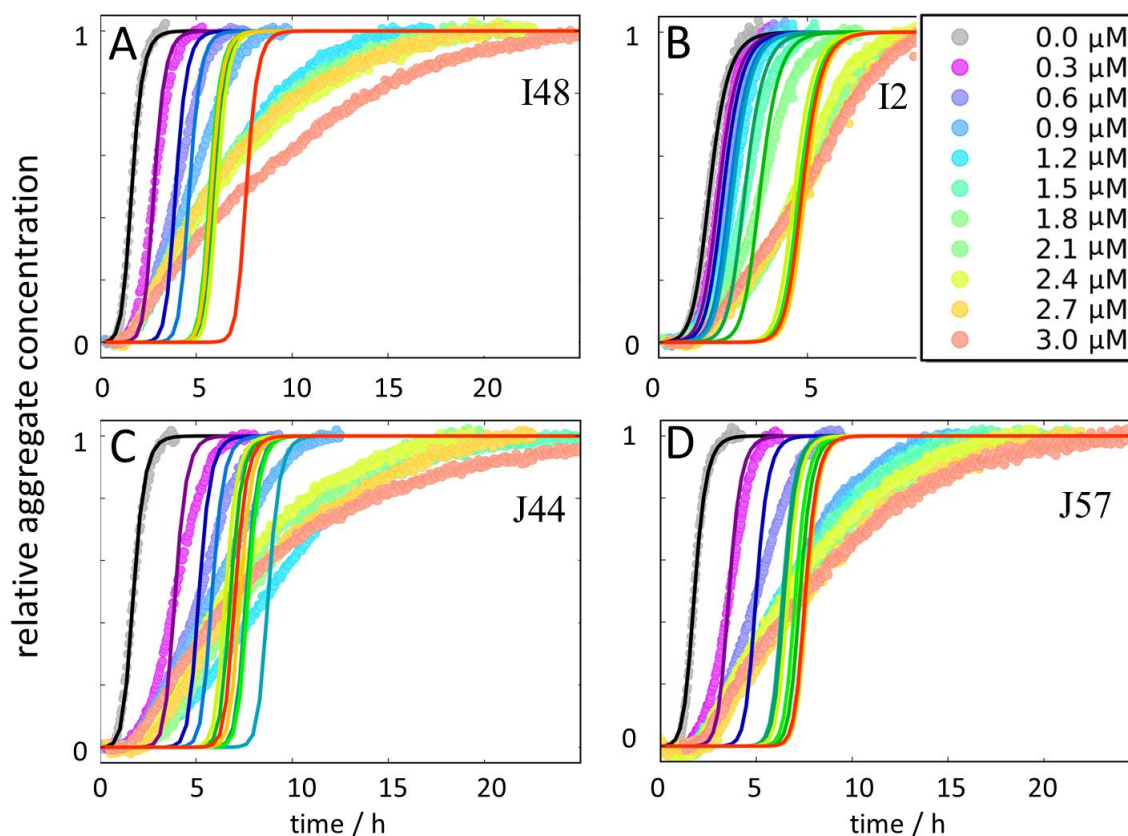


**Figure S2. Alternative kinetic analyses of scFvs found to selectively inhibit secondary nucleation.** Aggregation kinetics of solutions of 3  $\mu\text{M}$  A $\beta$ 42 monomer in the absence (black) and presence of four different scFvs from the phage display selection at concentrations ranging from 0.3 to 3.0  $\mu\text{M}$ : scFv-I48 (A), scFv-I2 (B), scFv-J44 (C) and scFv-J57 (D). The colour code for the data points is the same in all panels and is shown next to panel B. The fitted curves in panels A-D were generated by the AmyloFit interface<sup>28</sup> keeping  $k_+$  and  $k_2$  constant, while the rate constant  $k_n$  was allowed to take curve specific values at the different scFv concentrations.

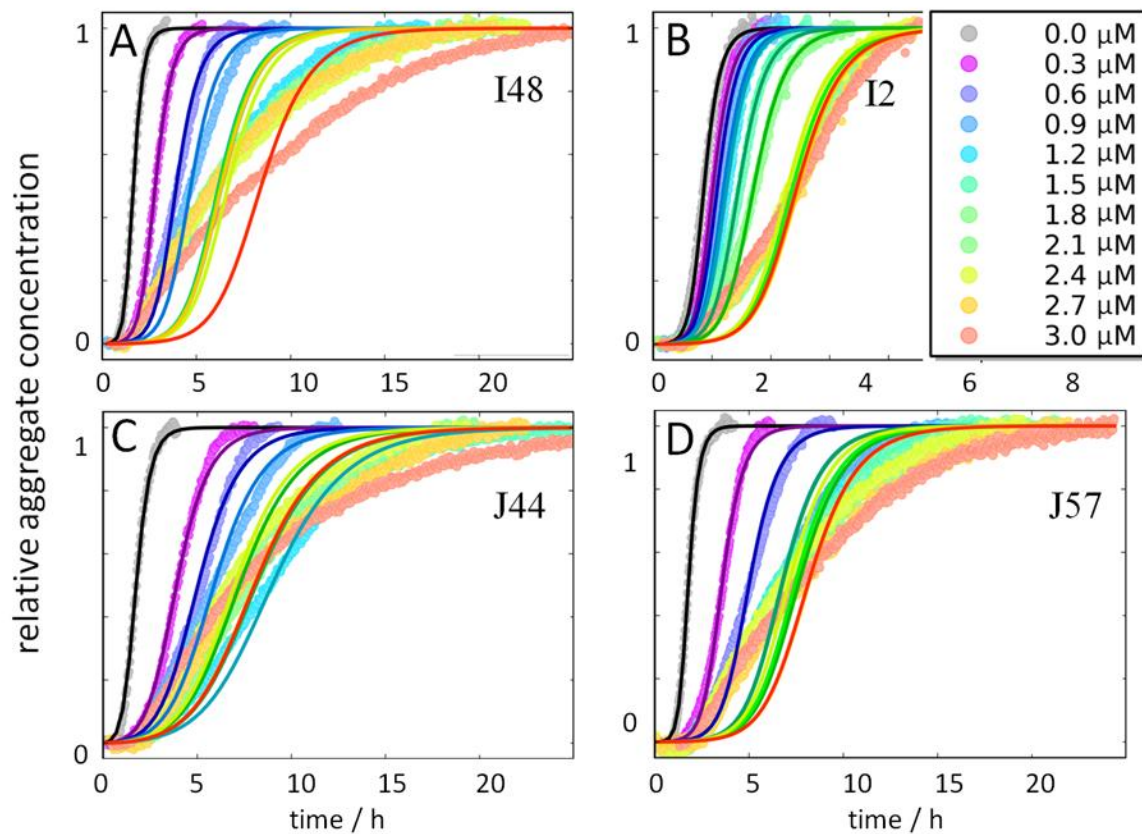
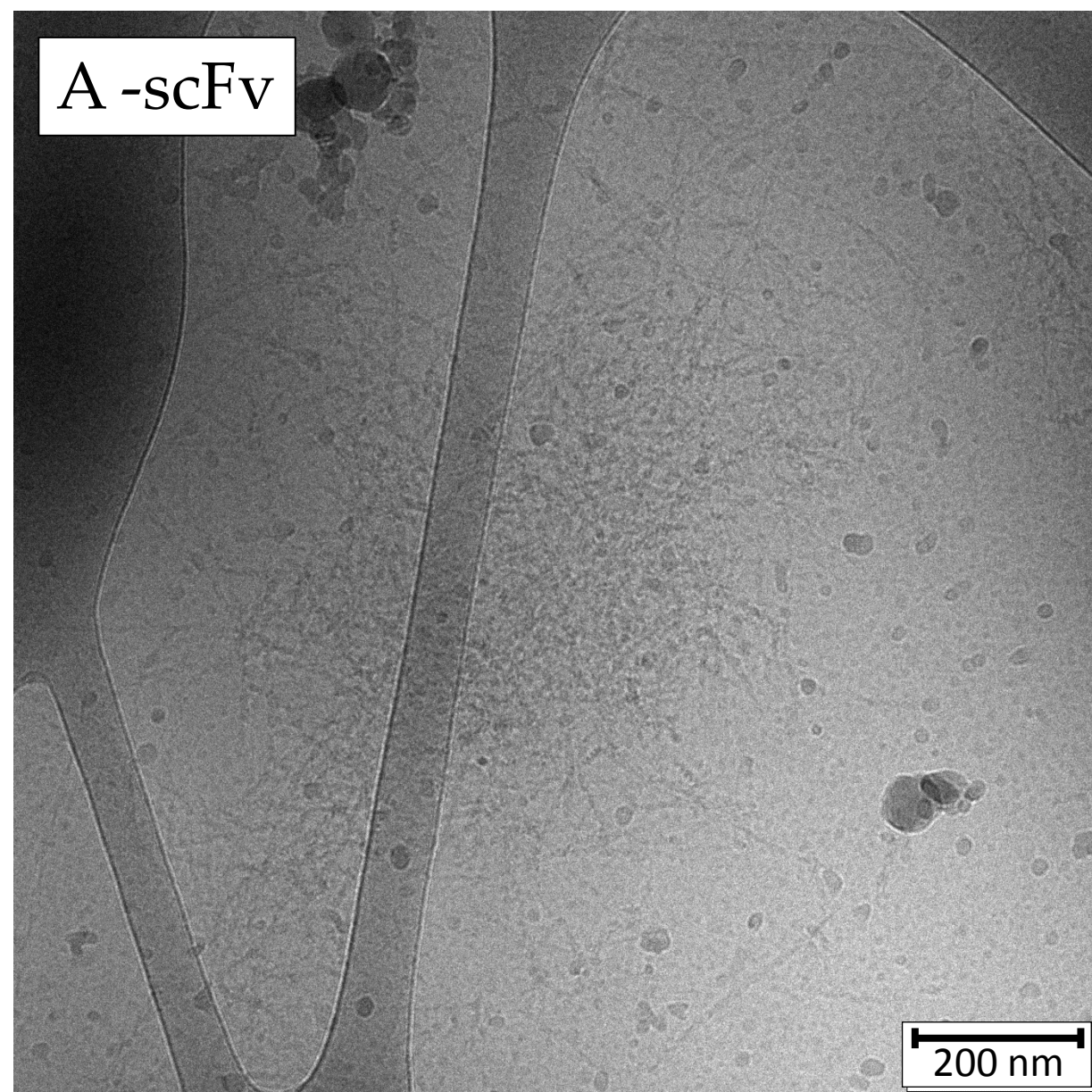


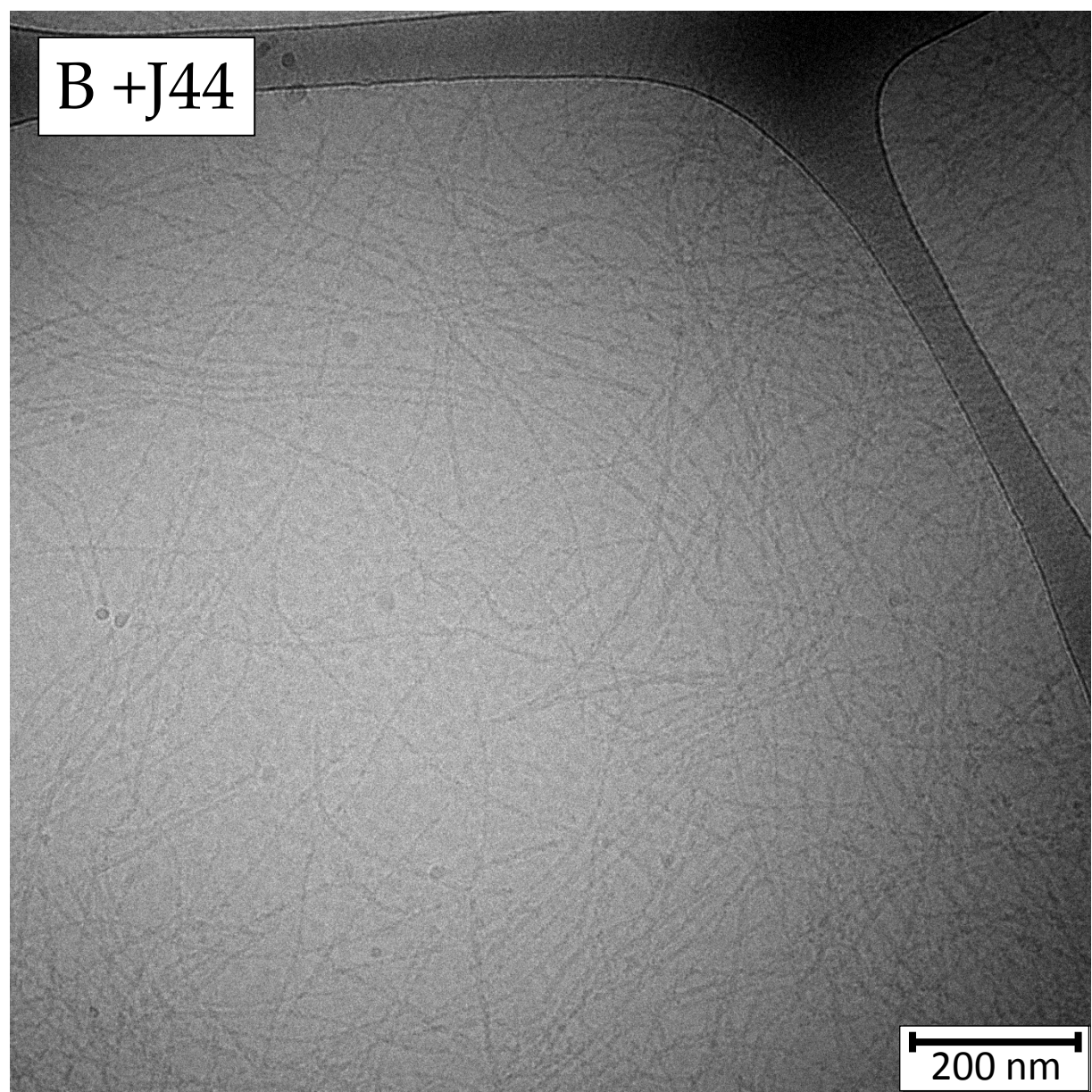
**Figure S3. Alternative kinetic analyses of scFvs found to selectively inhibit secondary nucleation.** Aggregation kinetics of solutions of 3  $\mu\text{M}$  A $\beta$ 42 monomer in the absence (black) and presence of four different scFvs from the phage display selection at concentrations ranging from 0.3 to 3.0  $\mu\text{M}$ : scFv-I48 (A,E), scFv-I2 (B,F), scFv-J44 (C,G) and scFv-J57 (D,H). The colour code for the data points is the same in all panels and is shown next to panel B. The fitted curves in panels A-D were generated by the AmyloFit interface<sup>28</sup> keeping  $k_n$  and  $k_2$  constant, while the rate constant  $k_+$  was allowed to take curve specific values at the different scFv concentrations.

**On next page: Figure S4. cryo-EM.** Cryo-EM images of fibrils fomred in *cryo*-TEM image of A $\beta$ 42 fibrils formed in the absence of scFv (A), or in the presence of scFv J44 (B), scFv I48 (C) or scFv I2 (D).

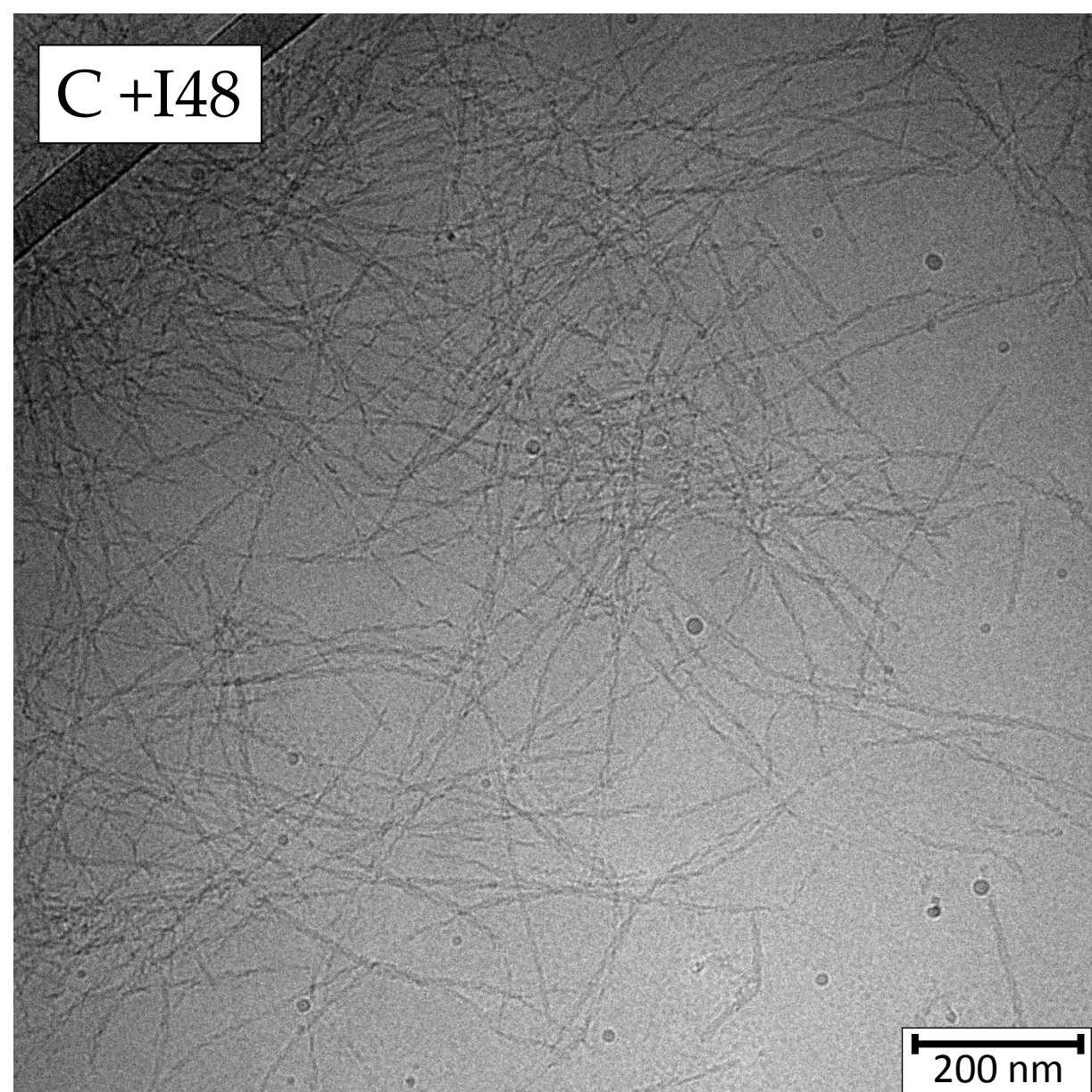
A -scFv



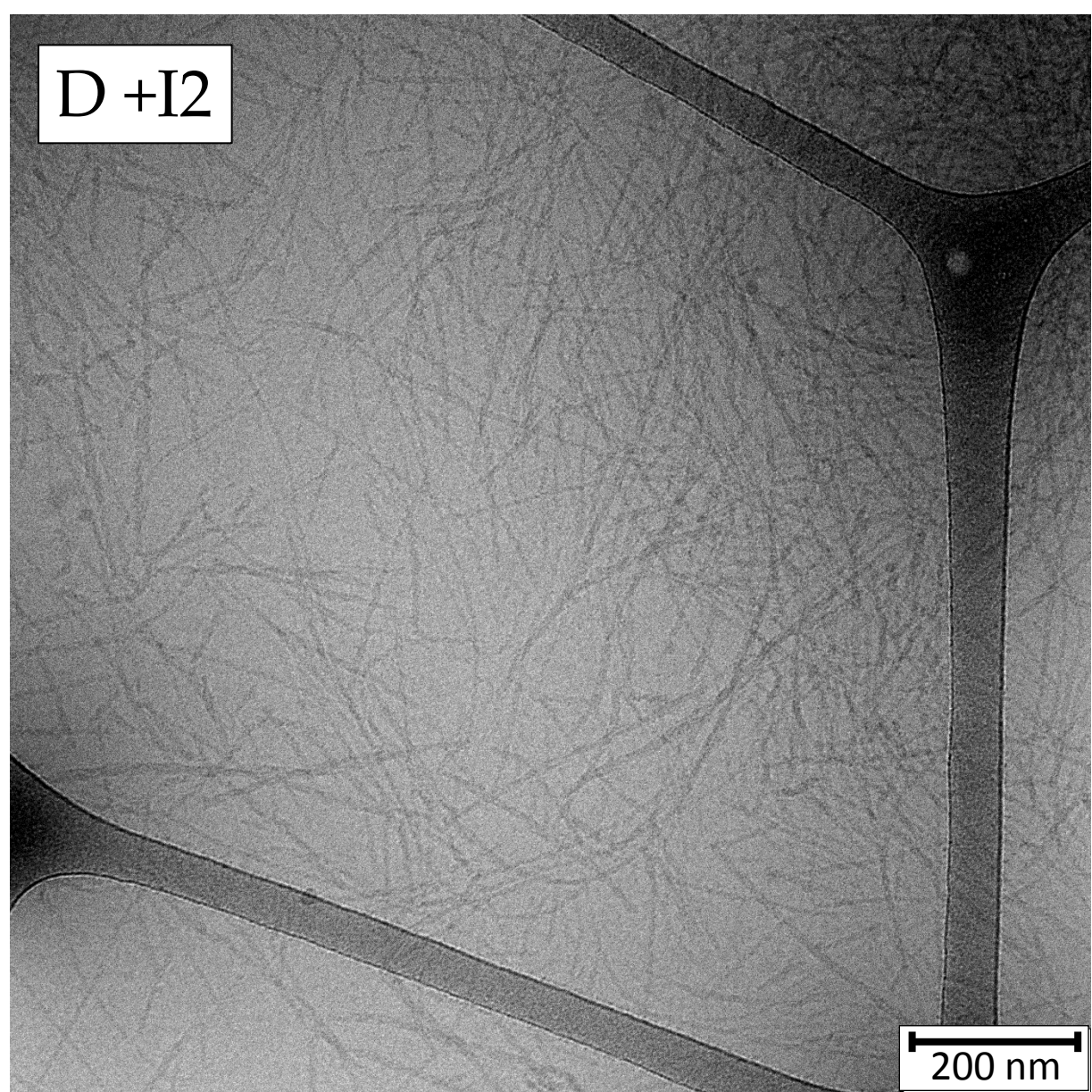
B +J44



C +I48



D +I2



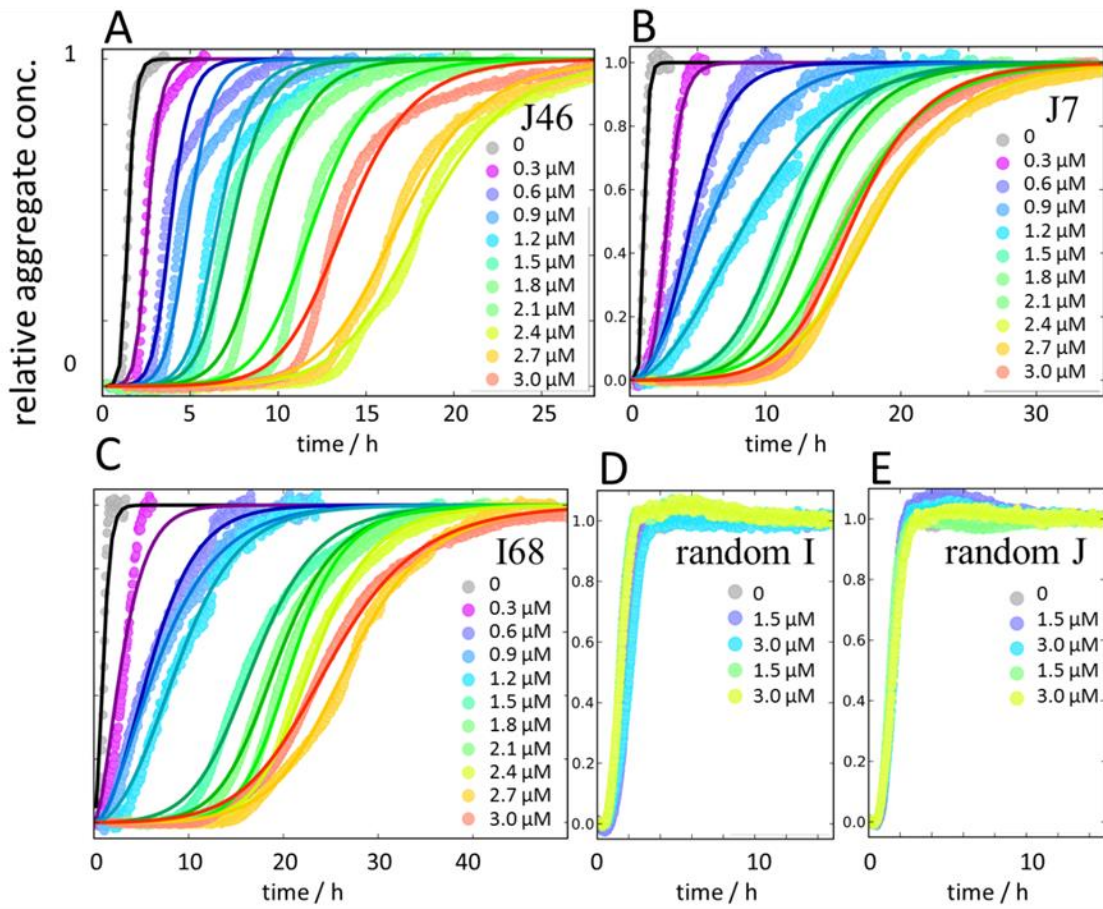


**Figure S5. Kinetic analyses of discarded scFvs that seem to inhibit elongation.** Aggregation kinetics of 3  $\mu\text{M}$  solutions of A $\beta$ 42 monomers in the absence (black) and presence of three different scFvs from the phage display selection at concentrations ranging from 0.3 to 3.0  $\mu\text{M}$ , and two control scFvs selected randomly from the I and J libraries. The fitted curves were generated by allowing both  $k_+k_n$  and  $k_+k_2$  to take curve-specific values at each scFv concentration.

## Epitope mapping fails to detect linear epitopes of the scFvs

**Membranes.** A SPOT-membrane (JPT Peptide Technologies GmbH Berlin, Germany) was designed with 33 different A $\beta$  peptides with lengths of 10 amino acids (Figure S6). Each spot contained about 5 nmol. The peptides were covalently bound by the C-terminus to a  $\beta$ Ala- $\beta$ Ala-anchor and prepared with an acetylated N-terminus. In addition, in-house spotted membranes were prepared by pipetting A $\beta$ 42 monomer or fibril solutions (10  $\mu$ M) on to a 0.20  $\mu$ m nitrocellulose membrane (LKB-produkter AB, Bromma) in drops of 5  $\mu$ L. Several droplets were deposited and allowed to dry in between. The spots of the in-house prepared membranes contained about 0.5 nmol A $\beta$ .

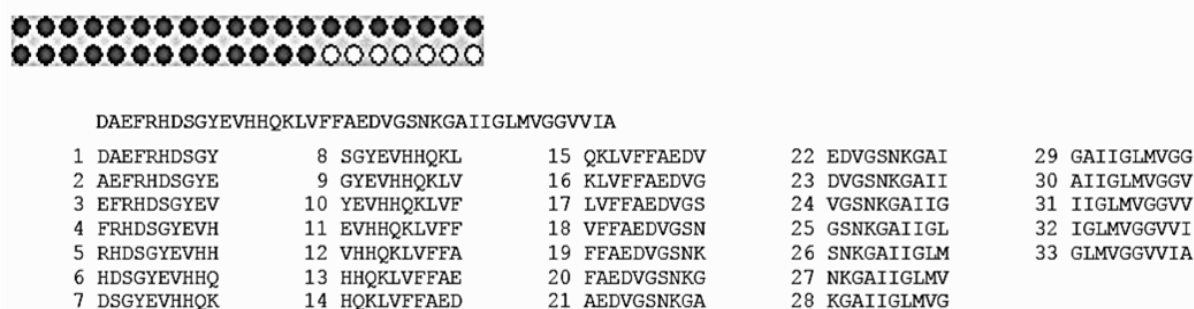


**Figure S6. Numbered sequence list and visualisation of the spot array.** 33 different 10 residues long peptides of the A $\beta$ 42 peptide were attached to the membrane, hence 9 residues were overlapping for spots next to each other.

**Fluorophore Labelling.** Protein A (a gift from Repligen Sweden AB, Lund, Sweden) and scFvs were labelled with IRDye® 800CW NHS ester infrared dye (LI-COR UK Ltd.) (MW=1166 Da) according to the manufacturer with following adjustments. Lyophilised dye was dissolved to 5 mg/ml in dimethyl sulfoxide (DMSO). The labelling reaction of protein A (MW=46762 Da) was carried out overnight at 4°C at a dye/protein ratio of 4:1 in PBS pH 8.5. The labelling reaction of scFv was carried out at room temperature (RT) for 2 hours at a dye/protein ratio of 3:1 in PBS pH 8.5.

**Dot blot Assay.** Binding between the scFvs and A $\beta$  was visualised using three different strategies: primary detection with labelled scFv; secondary detection with either a pre-labelled IRDye® 800CW goat anti-human IgG (LI-COR UK Ltd.) or labelled protein A (hereinafter named scFv<sup>IR</sup>, secondary Ab<sup>IR</sup> and protein A<sup>IR</sup>, respectively). The SPOT-membrane was activated by rinsing in methanol for 5 minutes and washed 3×10 minutes in TBS. Blocking was performed using 5% milk (skim milk powder, Fluka) in TBS pH 8.0 overnight at 4°C or for 2-3 hours at RT. All incubation steps, with scFv, secondary antibody or protein A, were performed by shaking in blocking solution for 2-3 hours at RT or overnight at 4°C. After each incubation step the membranes were washed for 3×5 minutes by shaking in TBS pH 8.0. Labelled proteins were incubated in dark. The following protein concentrations were used: 30-120  $\mu$ g/ml scFv, 1-9  $\mu$ g/ml scFv<sup>IR</sup>, 70 ng/ml secondary Ab<sup>IR</sup> and 1  $\mu$ g/ml protein A<sup>IR</sup>. The infrared dye was

detected with the 800 nm channel of ODYSSEY® CLx (LI-COR). Blocking, washing and incubation were performed in volumes of 20 ml.

A clear signal was detected at position 12 of the SPOT-membrane when incubating with scFv<sup>IR</sup>, as shown here for I68<sup>IR</sup> (Figure S7B). However, a signal was also detected at the same position for the secondary antibody (Figure S7A), indicating that the interaction may be with another part of the scFv rather than with the CDR loops.

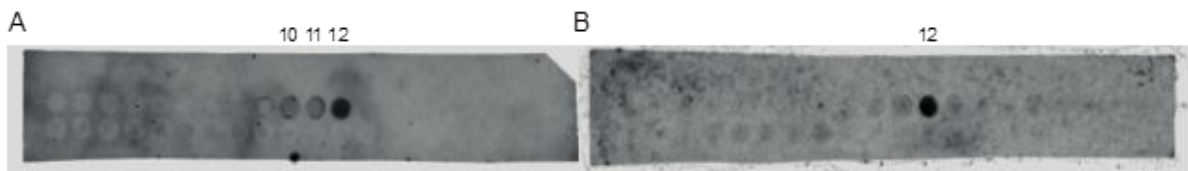


**Figure S7. Results from SPOT-membranes with 33 different A $\beta$  peptides.** A dark colour is visible where IRDye is detected. **A)** Negative control incubated with secondary Ab<sup>IR</sup>. The secondary Ab<sup>IR</sup> bind position 10-12, with highest signal from position 12. **B)** Incubating a SPOT-membrane with I68<sup>IR</sup> shows a strong signal at position 12.

In-house spotted membranes with A $\beta$ 42 monomers and fibrils were incubated either directly with I68<sup>IR</sup> (Figure S8A) or in two steps with I48 followed by protein A<sup>IR</sup> (Figure S8B). The binding of the scFvs to the fibrils was low but detectable. However, it is evident that the spots with fibrils are clearly different from the monomer spots, which have less signal than the background.

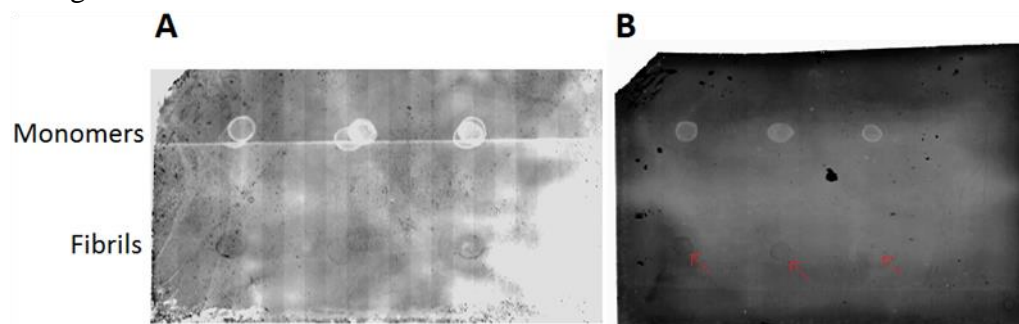


**Figure S8. Results from membranes spotted in-house with A $\beta$  monomers and fibrils.** Three spots of monomers and fibrils on each membrane on the upper respectively lower part of the membrane. A dark colour means that IRDye is detected. **A)** Primary detection with I68<sup>IR</sup>. More than one droplet of A $\beta$  was pipetted on each spot. **B)** Secondary detection of bound I48 with protein A<sup>IR</sup>. The red arrows help to point out the less detectable spots.

Altogether, these experiments failed to detect any linear epitopes for the scFvs comprising parts of the A $\beta$ 42 sequence. The only part of A $\beta$ 42 we cannot discuss is the peptide in spot 12, because this spot reacts with both scFvs and secondary antibodies.

## Supplementary references for text, figure captions and tables.

38. McCafferty J, Griffiths AD, Winter G, Chiswell DJ (1990) Phage antibodies: filamentous phage displaying antibody variable domains. *Nature*. 348:552-554.
39. Malmborg AC, Dueñas M, Ohlin M, Söderlind E, Borrebaeck CA (1996) Selection of binders from phage displayed antibody libraries using the BIAcore biosensor. *J Immunol Methods* 198:51-57.
40. Hellstrand E, Boland B, Walsh DM, Linse S (2010) Amyloid  $\beta$ -protein aggregation produces highly reproducible kinetic data and occurs by a two-phase process. *ACS Chem Neurosci* 1:13-18.
41. Kerchner, G. A. & Boxer, A. L. Bapineuzumab. *Expert Opin Biol Ther* **10**, 1121-1130 (2010).
42. *Alzforum: Clinical Trials of Intravenous Bapineuzumab Halted*, <http://www.alzforum.org/news/research-news/clinical-trials-intravenous-bapineuzumab-halted> (2013-12-23).
43. ClinicalTrials.gov  
<http://clinicaltrials.gov/ct2/results?term=Bapineuzumab&Search=Search>, (2016-04-25).
44. Delnomdedieu M, Duvvuri S, Li DJ, Atassi N, Lu M, Brashear HR, Liu E, Ness S and Kupiec JW. First-In-Human safety and long-term exposure data for AAB-003 (PF-05236812) and biomarkers after intravenous infusions of escalating doses in patients with mild to moderate Alzheimer's disease. *Alzheimers Res Ther* **8**:12 (2016)
45. ClinicalTrials.gov  
<http://clinicaltrials.gov/ct2/results?term=Gantenerumab&Search=Search>, (2016-04-25).
46. Novakovic, D. *et al.* Profile of gantenerumab and its potential in the treatment of Alzheimer's disease. *Drug Des Devel Ther* **7**, 1359–1364 (2013).
47. ClinicalTrials.gov  
<http://clinicaltrials.gov/ct2/results?term=Ponezumab&Search=Search>, (2016-04-25).
48. La Porte, S. L. *et al.* Structural Basis of C-terminal  $\beta$ -Amyloid Peptide Binding by the Antibody Ponezumab for the Treatment of Alzheimer's Disease. *J Mol Biol* **421**, 525-536 (2012).
49. Freeman, G. B., Lin, J. C., Pons, J. & Raha, N. M. 39-Week Toxicity and Toxicokinetic Study of Ponezumab (PF-04360365) in Cynomolgus Monkeys with 12-Week Recovery Period. *J Alzheimers Dis* **28**, 531-541 (2012).
50. <https://investor.lilly.com/releasedetail.cfm?ReleaseID=1000871>
51. Siemensa ER, Sundella KL, Carlsons C, Casea M, Sethuramana G, Liu-Seifert H, Dowsetta SA, Pontecorvob MJ, Deana RA, Demattosa R. Phase 3 solanezumab trials: Secondary outcomes in mild Alzheimer's disease patients. *Alzheimers Dement* **12**:110-120 (2016)
52. ClinicalTrials.gov  
<http://clinicaltrials.gov/ct2/results?term=Crenezumab&Search=Search>. (2016-04-27).
53. Garber, K. Genentech's Alzheimer's antibody trial to study disease prevention. *Nat Biotechnol* **30**, 731-732 (2012).
54. Jeffrey S. More positive data on aducanumab in Alzheimer's. *Medscape* May 11, (2015) <http://www.medscape.com/viewarticle/844502> (2016-04-21)
55. Keller DM. Finally, a big win for a monoclonal in Alzheimer's. *Medscape*. Mar 23, (2015) <http://www.medscape.com/viewarticle/841856> (2016-04-21)

56. ClinicalTrials.gov  
<https://clinicaltrials.gov/ct2/results?term=Aducanumab&Search=Search>
57. ClinicalTrials.gov. <http://clinicaltrials.gov/ct2/results?term=ban2401&Search=Search>, (2016-04-27).
58. Logovinsky V, Satlin A, Lai R, Swanson C, Kaplow J, Osswald G, Basun H and Lannfelt L. Safety and tolerability of BAN2401 - a clinical study in Alzheimer's disease with a protofibril selective A $\beta$  antibody. *Alzheimer's Research & Therapy* **8**:14 (2016)
59. Bard, F. *et al.* Peripherally administered antibodies against amyloid  $\beta$ -peptide enter the central nervous system and reduce pathology in a mouse model of Alzheimer disease. *Nat Med* **6**, 916-919 (2000).
60. Bard F, Barbour R, Cannon C, Carretto R, Fox M, Games D, Guido T, Hoenow K, Hu K, Johnson-Wood K, Khan K, Kholodenko D, Lee C, Lee M, Motter R, Nguyen M, Reed A, Schenk D, Tang P, Vasquez N, Seubert P, and Yednock T. Epitope and isotype specificities of antibodies to  $\beta$ -amyloid peptide for protection against Alzheimer's disease-like neuropathology. *PNAS* **100**: 2023–2028 (2003)
61. DeMattos, R. B. *et al.* Peripheral anti-A $\beta$  antibody alters CNS and plasma A $\beta$  clearance and decreases brain A $\beta$  burden in a mouse model of Alzheimer's disease *Proc Natl Acad Sci* **98**, 8850–8855 (2001)
62. Englund H, Sehlin D, Johansson AS, Nilsson LN, Gellerfors P, Paulie S, Lannfelt L, Pettersson FE. Sensitive ELISA detection of amyloid- $\beta$  protofibrils in biological samples. *J Neurochem* **103**:334-45 (2007)
63. Tucker S, Möller C, Tegerstedt K, Lord A, Laudon H, Sjö Dahl J, Söderberg L, Spens E, Sahlin C, Waara ER, Satlin A, Gellerfors P, Osswald G and Lannfelt L. The Murine Version of BAN2401 (mAb158) Selectively Reduces Amyloid- $\beta$  Protofibrils in Brain and Cerebrospinal Fluid of tg-ArcSwe Mice. *J Alzheimers Dis* **43**:575–588 (2015)
64. DeMattos, R. B. *et al.* A Plaque-Specific Antibody Clears Existing  $\beta$ -amyloid Plaques in Alzheimer's Disease Mice. *Neuron* **76**, 908-920 (2012).
65. Ying, Z. *et al.* Preparation and Characterization of a Monoclonal Antibody with High Affinity for Soluble Ab Oligomers. *Hybridoma (Larchmt)* **28**, 349-354 (2009).
66. Zhang, Y. *et al.* Administration of amyloid- $\beta$ 42 oligomer-specific monoclonal antibody improved memory performance in SAMP8 mice. *J Alzheimers Dis* **23**, 551-561 (2011).
67. Antonios G, Saiepour N, Bouter Y, Richard BC, Paetau A, Verkkoniemi-Ahola A, Lannfelt L, Ingelsson M, Kovacs GG, Pillot T, Wirths O and Bayer TA. N-truncated Abeta starting with position four: early intraneuronal accumulation and rescue of toxicity using NT4X-167, a novel monoclonal antibody. *Acta Neuropath Commun* 2013, **1**:56
68. Bouter Y, Lopez Noguerola JS, Tucholla P, Crespi GAN, Parker MW, Wiltfang J, Miles LA, Bayer TA. Abeta targets of the biosimilar antibodies of Bapineuzumab, Crenezumab, Solanezumab in comparison to an antibody against N-truncated Abeta in sporadic Alzheimer disease cases and mouse models. *Acta Neuropathol* **130**:713–729 (2015)
69. Yua YZ, Wanga WB, Chena A, Changa Q, Liua S, Zhaoa M, Wanga S, Qiu WY, Pangb XB, Xuc Q and Suna ZW. Strikingly Reduced Amyloid Burden and Improved Behavioral Performance in Alzheimer's Disease Mice Immunized with Recombinant Chimeric Vaccines by Hexavalent Foldable A $\beta$ 1-15 Fused to Toxin-Derived Carrier Proteins. *J Alzheimers Dis* **41**:243–260 (2014)
70. Wanga HC, Yub YZ, Liub S, Zhaoa M, Xua Q. Peripherally administered sera antibodies recognizing amyloid- $\beta$  oligomers mitigate Alzheimer's disease-like pathology and cognitive decline in aged 3 $\times$  Tg-AD mice. *Vaccine* **34**:1758–1766 (2016)
71. Skaat, H. *et al.* Antibody-conjugated, dual-modal, near-infrared fluorescent iron oxide nanoparticles for anti-amyloidogenic activity and specific detection of amyloid- $\beta$  fibrils. *Int J Nanomedicine* **8**, 4063-4076 (2013).

72. Wang T, Xie XX, Ji M, Wang SW, Zha J, Zhou WW, Yu XL, Wei C, Ma S, Xi ZY, Pang GL, Liu RT. Naturally occurring autoantibodies against Ab oligomers exhibited more beneficial effects in the treatment of mouse model of Alzheimer's disease than intravenous immunoglobulin. *Neuropharmacology* **105**:561e576 (2016)
73. Bodani RU, Sengupta U, Castillo-Carranza DL, Guerrero-Muñoz MJ, Gerson JE, Rudra J, and Kaye R. Antibody against Small Aggregated Peptide Specifically Recognizes Toxic A $\beta$ -42 Oligomers in Alzheimer's Disease. *ACS Chem Neurosci* **6**:1981-9 (2015)
74. Levites Y, O'Nuallain B, Puligedda RD, Ondrejcek T, Adekar SP, Chen C, Cruz PE, Rosario AM, Macy S, Mably AJ, Walsh DM, Vidal R, Solomon A, Brown D, Rowan MJ, Golde TE, and Dessain SK. A Human Monoclonal IgG That Binds A $\beta$  Assemblies and Diverse Amyloids Exhibits Anti-Amyloid Activities In Vitro and In Vivo. *J Neurosci* **35**:6265-76 (2015)
75. Liu, R. *et al.* Single Chain Variable Fragments against  $\beta$ -Amyloid (A $\beta$ ) Can Inhibit A $\beta$  Aggregation and Prevent A $\beta$ -Induced Neurotoxicity. *Biochemistry* **43**, 6959-6967 (2004).
76. Zameer, A., Schulz, P., Wang, M. S. & Sierks, M. R. Single chain Fv antibodies against the 25-35 Abeta fragment inhibit aggregation and toxicity of Abeta42. *Biochemistry* **45**, 11532-11539 (2006).
77. Yoshihara, T. *et al.* Immunoreactivity of phage library-derived human single-chain antibodies to amyloid beta conformers in vitro. *J Biochem* **143**, 475-486 (2008).
78. Wang J, Li N, Ma J, Gu Z, Yu L, Fu X, Liu X, Wang J. Effects of an amyloid-beta 1-42 oligomers antibody screened from a phage display library in APP/PS1 transgenic mice *Brain Res* **1635**:169-79 (2016)
79. Zhang Y, Sun Y, Huai Y, Zhang YJ. Functional Characteristics and Molecular Mechanism of a New scFv Antibody Against A $\beta$ 42 Oligomers and Immature Protofibrils. *Mol Neurobiol* **52**:1269-81 (2015)
80. Tammer AH, Coia G, Cappai R, Fuller S, Masters CL, Hudson P, Underwood JR. Generation of a recombinant Fab antibody reactive with the Alzheimer's disease-related A $\beta$  peptide. *Clin Exp Immunol* **129**:453-63 (2002)
81. Nisbet RM, Nigro J, Breheney K, Caine J, Hattarki MK, Nuttall SD. Central amyloid- $\beta$ -specific single chain variable fragment ameliorates A $\beta$  aggregation and neurotoxicity. *Protein Eng Des Sel* **26**:571-80 (2013)
82. Wang, X. P. *et al.* Conformation-dependent single-chain variable fragment antibodies specifically recognize beta-amyloid oligomers. *FEBS Lett* **583**, 579-584 (2009).
83. Zhang, X. *et al.* Conformation-dependent scFv antibodies specifically recognize the oligomers assembled from various amyloids and show colocalization of amyloid fibrils with oligomers in patients with amyloidoses. *Biochim Biophys Acta* **1814**, 1703-1712 (2011).
84. Taguchi H, Planque S, Sapparapu G, Boivin S, Hara M, Nishiyama Y, Paul S. Exceptional Amyloid  $\beta$  Peptide Hydrolyzing Activity of Nonphysiological Immunoglobulin Variable Domain Scaffolds. *J Biol Chem* **283**:36724-33 (2008)
85. Planque SA, Nishiyama Y, Sonoda S, Lin Y, Taguchi H, Hara M, Kolodziej S, Mitsuda Y, Gonzalez V, Sait HBR, Fukuchi K, Massey RJ, Friedland RP, O'Nuallain B, Sigurdsson EM, Paul S. Specific Amyloid  $\beta$  Clearance by a Catalytic Antibody Construct *J Biol Chem* **290**:10229-41 (2015)
86. O'Nuallain, B. & Wetzel, R. Conformational Abs recognizing a generic amyloid fibril epitope. *Proc Natl Acad Sci U S A* **99**, 1485-1490 (2002).
87. Morgado, I. *et al.* Molecular basis of  $\beta$ -amyloid oligomer recognition with a conformational antibody fragment. *Proc Natl Acad Sci U S A* **109**, 12503-12508 (2012).

88. Habicht, G. *et al.* Directed selection of a conformational antibody domain that prevents mature amyloid fibril formation by stabilizing A $\beta$  protofibrils. *Proc Natl Acad Sci* **104**, 19232-19237 (2007).
89. Haupt, C. *et al.* Amyloid Fibril Recognition with the Conformational B10 Antibody Fragment Depends on Electrostatic Interactions. *J Mol Biol* **405**, 341-348 (2011).
90. Lafaye, P., Achour, I., England, P., Duyckaerts, C. & Rougeon, F. Single-domain antibodies recognize selectively small oligomeric forms of amyloid beta, prevent Abeta-induced neurotoxicity and inhibit fibril formation. *Mol Immunol* **46**, 695-704 (2009).
91. Perchiacca, J. M., Ladiwala, A. R., Bhattacharya, M. & Tessier, P. M. Structure-based design of conformation- and sequence-specific antibodies against amyloid  $\beta$ . *Proc Natl Acad Sci U S A* **109**, 84-89 (2012).
92. Boado, R. J., Zhang, Y., Zhang, Y., Xia, C. F. & Pardridge, W. M. Fusion antibody for Alzheimer's disease with bidirectional transport across the blood-brain barrier and abeta fibril disaggregation. *Bioconjug Chem* **18**, 447-455 (2007).

**Table S1. Previously reported anti-A $\beta$  antibodies divided into 6 sub-categories: 1. Clinically tested antibodies; 2. IgG antibodies; 3. ScFv's; 4. IgM antibody; 5. Camelid antibodies; and 6. Special antibody formats.** Numerous anti-A $\beta$  antibodies are reported and the aims and questions addressed in these studies vary. For each antibody, following information is presented (if published): *Origin* (how it was obtained), *Antibody construct* (antibody class/subclass; monoclonal/polyclonal; its source, e.g. humanized, chimeric; and type, e.g. IgG, scFv), *Binding capacity*, *Epitope* and *Main results*. IgGs and scFvs are considered to be approximately 150 kDa and 25-29 kDa respectively. Approximate molecular weights are given for all other antibody types.

Antibody	Origin	Antibody construct	Binding capacity	Epitope	Main results	Additional comment	Ref.
<b>1. Clinically tested antibodies</b>							
<b>Bapineuzumab</b>	Raised in mice against A $\beta$ residues 1-5.	Monoclonal humanized murine <b>3D6</b> IgG1	Bind amyloid plaques more strongly than soluble A $\beta$ .	N-terminus ~1-5	No effect on cognitive abilities. Side effect: primary vasogenic cerebral edema.	First anti-A $\beta$ antibody that was clinically tested (2005). Phase 3 (intravenous administrated) halted in August 2012. (Sponsor: Janssen/Pfizer)	41-43
<b>AAB-003</b>	Raised in mice against A $\beta$ residues 1-5.	Monoclonal humanized murine <b>3D6</b> IgG1	Bind amyloid plaques more strongly than soluble A $\beta$ .	N-terminus ~1-5	ARIA-E <sup>1</sup> was observed at a higher dose than Bapineuzumab.	Modified Bapineuzumab with aim of reducing ARIA-E. (Sponsor: Janssen/Pfizer)	44
<b>Gantenerumab</b>	Selected from a synthetic human library based on phage display technology.	Monoclonal human IgG1	Highest affinity to fibrils, less to monomers.	Target the N-terminus and central portion of A $\beta$ .	Phase 1 study of 16 AD patients treated for a short period of time resulted in a dose-dependent reduction in brain amyloid level but no consistent treatment effects on cognitive endpoints were revealed.	Library: HuCAL@; MorphoSys Martinsried/Planegg, Germany. Phase 2 & 3 clinical trials are ongoing and estimated to be completed during 2016. First entirely human anti-A $\beta$ monoclonal antibody to enter clinical development. (Sponsor: Hoffmann-La Roche).	45,46

<sup>1</sup> Amyloid related imaging abnormalities, E stands for edema

Antibody	Origin	Antibody construct	Binding capacity	Epitope	Main results	Additional comment	Ref.
<b>Ponezumab</b>	Raised in mice. Antigenic target not published.	Monoclonal humanized murine IgG2Δa (IgG2 with Fc region containing two mutations)	Bind monomeric, oligomeric and fibrillar forms of Aβ40 equally well. No binding to any form of Aβ42.	C-terminus of Aβ40, ~30–40.	Early clinical findings demonstrated that Ponezumab is well tolerated in monkeys.  Hypothesised to possess a mechanism that shifts the Aβ brain-blood equilibrium towards the blood.	Phase 2 completed. Fc region contains two mutations that eliminate effector function. (Sponsor: Pfizer)	47-49
<b>Solanezumab</b>	Raised in mice against Aβ residues 13-28.	Monoclonal humanized murine <b>m266</b> IgG1	Selectively bind to soluble Aβ with little to no affinity for the fibrillar form.	Mid-terminus (~13-28)	Patients treated with Solanezumab did not experience a statistically significant slowing in cognitive decline compared to patients treated with placebo.	(Sponsor: Eli Lilly)	50,51
<b>Crenezumab</b>	Antigenic target not published.	Monoclonal humanized IgG4	Target monomers, oligomers and fibrils.	Aβ12-23	In July 2012 more than 250 patients had received Crenezumab with no reported cases of treatment related vasogenic edema or microhemorrhage.	The first clinical trial of a drug's ability to forestall AD in cognitively healthy individuals. The IgG4 backbone serves to limit microglial activation, a likely contributor to vasogenic edema. Currently recruiting for its first phase 3 trial. (Sponsor: Genentech/Hoffmann-La Roche)	52,53
<b>Aducanumab</b>	Replica of an anti-Aβ IgG isolated from healthy, aged donors who were cognitively normal.	Monoclonal human IgG1	Bind aggregated forms of Aβ, not monomers.	Aggregated Aβ	Phase 1 study showed a dose-dependent clearance of plaque and an improvement of cognition.	The mechanism of action is thought to be microglial-mediated phagocytosis and clearance of Aβ through the IgG1 backbone. Currently recruiting in phase 3 trial. (Sponsor: Biogen)	54-56
<b>BAN2401</b>	Its murine precursor, mAb158, was raised in mice against Aβ1–42Arc protofibrils	Monoclonal humanized IgG1	Target Aβ protofibrils	Conformational, N-terminal	The incidence of ARIA-E/H <sup>2</sup> on MRI was comparable to that of placebo. It entered the CSF and showed dose-dependent exposure.	Phase 1 to study safety and tolerability is completed and recruiting is currently ongoing for a phase 2 study. (Sponsor: Eisai/BioArctic Neuroscience)	57,58

<sup>2</sup> Amyloid related imaging abnormalities, E stands for edema and H for hemorrhage

Antibody	Origin	Antibody construct	Binding capacity	Epitope	Main results	Additional comment	Ref.
<b>2. IgG antibodies</b>							
<b>16C11</b>	Raised in mice. A $\beta$ species not published.	Monoclonal murine IgG1	Binds aggregated synthetic A $\beta$ peptide with high avidity, but are unable to bind plaques in unfixed brain sections. Also bind soluble A $\beta$ .	C-terminus (~33-42)	Antibodies 10D5, 3D6 and pabA $\beta$ (1-42) were all active in the <i>ex vivo</i> assay (induced phagocytosis of AD plaques) and demonstrated efficacy <i>in vivo</i> (reduced plaque burden by greater than 80%, 86% and 93% respectively). 16C11 and 21F12 were inactive in both assays.	First preclinical study on passive immunotherapy. 3D6 is the murine equivalent of Bapineuzumab.	59,60
<b>21F12</b>	Raised in mice against A $\beta$ 33-42.	Monoclonal murine IgG2a					
<b>pabA<math>\beta</math>(1-42)</b>	Raised in mice against the entire A $\beta$ 42 peptide	Polyclonal murine	Bind plaques. Other species not investigated.	N-terminal			
<b>3D6</b>	Raised in mice against A $\beta$ 1-5.	Monoclonal murine IgG2a	Bind plaque. Bind soluble A $\beta$ with low affinity.	N-terminus (~1-5)			
<b>10D5</b>	Raised in mice against A $\beta$ 1-28	Monoclonal murine IgG1	Bind plaque. Low or no affinity for soluble A $\beta$ .	N-terminus (~3-7)			
<b>m266</b>	Raised in mice against A $\beta$ 13-28	Monoclonal murine IgG, isotype not published	Selectively bind to soluble A $\beta$ . Does not bind plaque.	Mid-terminus (~13-28)			

Antibody	Origin	Antibody construct	Binding capacity	Epitope	Main results	Additional comment	Ref.
<b>mAb158</b>	Raised in mice against A $\beta$ 1–42Arc protofibrils	Monoclonal murine IgG2a	Preferably bind protofibrils (A $\beta$ 42 and A $\beta$ Arc equally well). Some binding affinity to LMW-A $\beta$ <sup>3</sup> and A $\beta$ 1-16. Does not bind APP <sup>4</sup> .	Conformational, N-terminal. Does not recognize a generic amyloid epitope.	mAb158 reaches the brain of mice and reduce especially A $\beta$ protofibril levels, but also the total A $\beta$ 42 levels.	The Arctic mutation: A $\beta$ E22G, which causes enhanced formation of A $\beta$ protofibrils (oligomeric A $\beta$ species of >100 kDa) <i>in vitro</i> . Murine equivalent of BAN2401.	62,63
<b>mE8</b>	Raised in mice against modified A $\beta$ , A $\beta$ (p3-X)	Monoclonal murine IgG, (constructed as both IgG1 and IgG2a isotypes)	Plaque specific	Modified N-terminus of A $\beta$ (p3-X) (does not recognize full-length A $\beta$ or unmodified A $\beta$ (3-x))	Both isotypes facilitate clearance of deposited plaque <i>ex vivo</i> . The mE8-IgG1 and mE8-IgG2a lowered the Ab42 by 38% and 53%, respectively.	Comparison with 3D6: proposed a preventative action for 3D6 as oppose to mE8 that is more efficient in clearing plaques.	64
<b>A8</b>	Raised in mice against A $\beta$ 42 oligomers	Murine monoclonal IgG2b	Predominantly bind soluble oligomers in the 16.5–25 kDa range.	N-terminus (within residues 1-6)	Suppresses A $\beta$ aggregation and cell toxicity. Improves spatial memory and A $\beta$ pathology.	-	65,66
<b>NTX4-167</b>	Raised in mice against A $\beta$ 4–40	Monoclonal murine IgG2b	Oligomers. Minor binding activity to plaques. Does not bind full length A $\beta$ . Does not bind A $\beta$ 36–40.	A $\beta$ 4–40 for immunization and further screening for binding to A $\beta$ 4–10, A $\beta$ 4–40	Showed vascular binding activity in 32 of 35 cases of SAD <sup>5</sup> . Did not cross-react with other amyloid aggregates than A $\beta$ 4–42 in brain tissue sections.	Reference 28 performed comparable studies with Bapineuzumab, Crenezumab and Solanezumab	67,68
<b>Anti-6A<math>\beta</math>15-T serum antibodies</b>	Sera obtained through immunization of 6A $\beta$ 15-T (hexavalent foldable A $\beta$ 1-15)	Murine and rabbit IgG serum	Recognize A $\beta$ 42 monomers and oligomers.	Within the A $\beta$ 1-15 region	Reduced amyloid burden, improved behavioural performance in mice and prevented degradation of dynamin 1.	-	69,70
<b>BAM10-conjugated nanoparticles</b>	Raised in mice against A $\beta$ 40	Monoclonal murine IgG1	Bind plaques. Other species not examined.	N-terminus (within residues 1-12)	Inhibits A $\beta$ 40 fibrillation in contrast to BAM10 and nanoparticles alone. Also enabled specific detection of A $\beta$ 40 fibrils <i>ex vivo</i> .	Conjugated to NIR fluorescent maghemite ( $\gamma$ -Fe <sub>2</sub> O <sub>3</sub> ) nanoparticles. BAM10 is commercially available from Sigma-Aldrich.	71

<sup>3</sup> Low molecular weight (LMW) A $\beta$  are monomers-tetramers of 4-20 kDa

<sup>4</sup> Amyloid precursor protein

<sup>5</sup> Sporadic Alzheimer's disease

Antibody	Origin	Antibody construct	Binding capacity	Epitope	Main results	Additional comment	Ref.
<b>Oli-NAbs and Blue-NAbs</b>	Isolated from IVIG by using A $\beta$ 42 oligomers (Oli-NAbs) or Cibacron Blue (Blue-NAbs) affinity chromatography.	IgG	Blue-NAbs recognise A $\beta$ 40 and 42 oligomers rather than their monomers or fibrils. Oli-NAbs mainly bind A $\beta$ 42 oligomers rather than A $\beta$ 40 oligomers or their monomers and fibrils.	Conformational: oligomers	Inhibits A $\beta$ 42 aggregation. Improves cell viability. Rescues memory deficits and synaptic dysfunction in AD transgenic mice. Reduces plaque and oligomers in mice brain. Does not induce microhemorrhages and T cell infiltration.	-	72
<b>VIA</b>	Raised in rabbit against VIAVIA peptide.	Rabbit IgG serum	Oligomers of A $\beta$ 42. Does not recognize plaques <i>ex vivo</i> .	Peptides of the last three amino acids in A $\beta$ 42 (Val-40, Ile-41 and Ala-42) in the form of aggregated VIAVIA.	Results indicate that VIA reduces the toxic effect of A $\beta$ 42 oligomers.	-	73
<b>3H3</b>	IgG isolated from memory B cells of a healthy subject by screening with A $\beta$ 40 or JTO6 fibrils. scFv was recombinantly expressed.	Human monoclonal IgG and scFv.	Binding investigated with various A $\beta$ 40 conformers and found to preferably bind aggregated forms.	Pan-amyloid conformers, recognising both A $\beta$ and $\lambda$ Ig light chain aggregates (ELISA and brain tissue).	Inhibits A $\beta$ and $\lambda$ Ig light chain aggregation <i>in vitro</i> . Reduce synaptic plasticity in the hippocampus caused by A $\beta$ oligomers. When scFv was expressed in the brains of transgenic mice using an adeno-associated virus (AAV) vector, the parenchymal A $\beta$ amyloid deposition and ADan (Danish Amyloid) cerebral amyloid angiopathy in mice decreased.	-	74

<sup>6</sup> Recombinant amyloidogenic  $\lambda$ 6 LC variable region cloned from a multiple myeloma patient

Antibody	Origin	Antibody construct	Binding capacity	Epitope	Main results	Additional comment	Ref.
<b>3. ScFv's</b>							
<b>H1v2, C1</b>	Recombinant selected from a synthetic human phage display library: H1v2 against residues 1-28 and further affinity matured against A $\beta$ 40 and C1 against A $\beta$ 40.	Human scFv	Monomers (did not test other species)	H1v2 bind somewhere between residues 17-28 and C1 bind somewhere between residues 29-40.	H1v2 inhibits aggregation while C1 has little effect. H1v2 can provide protection from toxicity and C1 can provide partial protection.	Library obtained from the Medical Research Council (Cambridge, England)	75
<b>B6, D4</b>	Recombinant, selected from a naïve human phage display library against A $\beta$ 25-35.	Human scFv	Bind A $\beta$ 40, A $\beta$ 42 and A $\beta$ 25-35 (A $\beta$ assembly not reported). D4 higher affinity for A $\beta$ 40, B6 higher affinity for A $\beta$ 25-35.	Not published	ThT fluorescence and AFM shows inhibition of A $\beta$ 42 aggregation. Are able to dissolve preformed aggregates to some extent. Blocked A $\beta$ 42 toxicity.	Tomlinson I and J library. Not the same research group as ref 37.	76
<b>B6</b>	Recombinant, selected against A $\beta$ 42 fibrils from a human phage display library generated in house.	Human scFv	Binds A $\beta$ 42 fibrils and oligomers but not monomers.	C-terminus	scFvs selected against A $\beta$ 42 fibrils (including B6) inhibit A $\beta$ 42 fibrillation markedly, as opposed to the monomer selected that hardly showed any inhibitory effect.	First human inhibitory antibody recognizing the C-terminus. Reported on additional 8 scFv's, but focused on B6. Not the same research group as ref. 36.	77
<b>11A5</b>	Recombinant, selected based on its specificity for A $\beta$ 42 oligomers.	Human scFv	A $\beta$ 42 oligomers	A $\beta$ 42 oligomers	Decreased neurotoxic effects on rats. Improvement in learning abilities and memory of mice. Suggested mechanism of action: initiates A $\beta$ efflux or clearance from the brain to the peripheral blood.	Selected from a library constructed by extracting lymphocyte RNA from blood from AD patients.	78

Antibody	Origin	Antibody construct	Binding capacity	Epitope	Main results	Additional comment	Ref.
<b>AS</b>	Recombinant, selected against A $\beta$ 42 oligomers from a library generated by isolating leukocytes from peripheral blood of AD patients.	Human scFv	A $\beta$ 42 oligomers as well as immature protofibrils (25– 55 kDa), but not to A $\beta$ 42 monomers and fibrils.	A $\beta$ 42 oligomers	Inhibits A $\beta$ 42 aggregation (ThT fluorescence). Protects SH-SY5Y cells against A $\beta$ 42 cytotoxic effects in a concentration dependent manner.	-	79
<b>1E8</b>	Recombinant	Murine scFv derived from the Fab sequence of the IgG variant of 1E8.	A $\beta$ monomers, and peptides containing residues 17-22. Engineering into scFv did not alter binding efficiency and specificity.	A $\beta$ 17-22	Inhibits A $\beta$ 42 aggregation (ThT fluorescence) and prevents cytotoxic effects <i>in vitro</i> .	-	80,81
<b>W8, W20</b>	Recombinant, selected against A $\beta$ 42 oligomers selected from a naïve human phage display library.	Human scFv	Recognise A $\beta$ 42 oligomers but not monomers or fibrils. Recognise amyloids oligomers assembled from $\alpha$ -synuclein, IAPP <sup>7</sup> , insulin, lysozyme, A $\beta$ 40 and PrP <sup>8</sup> 106–126. Recognise lysozyme fibrils.	Bind the same type of epitope displayed on the A $\beta$ oligomers. The exact location not published.	Inhibits A $\beta$ 42 fibrillation and cytotoxicity. Dissolves preformed aggregates. Inhibits aggregation of $\alpha$ -synuclein, amylin, insulin, A $\beta$ 40 and PrP to various extents. However, lysozyme fibril formation was promoted by the scFv's.	Tomlinson I and J library. Reported additional 2 scFv's (W8 and W20 had the highest affinity).	82,83

<sup>7</sup> Islet Amyloid Polypeptide (or amylin)

<sup>8</sup> Prion protein

Antibody	Origin	Antibody construct	Binding capacity	Epitope	Main results	Additional comment	Ref.
2E6	Recombinant, selected from an IgV library based on screening with electrophilic Bt-E-A $\beta$ 40 <sup>9</sup>	Human catabody <sup>10</sup> . Two heterodimeric V <sub>L</sub> chains linked together.	-	C terminus	2E6 had the highest <sup>125</sup> I-A $\beta$ 40 hydrolyzing activity of initially selected antibodies. Prefibrillated A $\beta$ 42 are nearly completely dissolved. Inhibits aggregation more strongly than an A $\beta$ -binding IgG. Reduce brain A $\beta$ deposits in a mouse model without inducing microgliosis or microhemorrhages.	IgV library: derived from peripheral blood lymphocytes of three lupus patients without amyloid disease.	84,85
<b>4. IgM antibody</b>							
WO1, WO2	Raised in mice against sonicated A $\beta$ 40 fibrils	Monoclonal murine IgM, ~900 kDa	Bind amyloid fibrils or amyloid-like aggregates composed of A $\beta$ 40, $\beta$ 2m <sup>11</sup> , IAPP <sup>12</sup> , TTR <sup>13</sup> , polyGln (Q42) <sup>14</sup> , the Ig V <sub>L</sub> domain JTO5 and lysozyme. However, exhibits maximal binding to A $\beta$ 40 fibrils. Do not recognize A $\beta$ 40 monomers.	Conformational	Only the binding capacity was studied.	-	86

<sup>9</sup> Two electrophilic phosphate *diphenyl-N-[O-(3-sulfosuccinimidyl)suberoyl]-amino(4-amidinophenyl) methane phosphonate* incorporated between A $\beta$ 15-16 and A $\beta$ 26-27 respectively.

<sup>10</sup> Catalytic antibody

<sup>11</sup>  $\beta$ 2 microglobulin

<sup>12</sup> Islet Amyloid Polypeptide (or amylin)

<sup>13</sup> Transthyretin

<sup>14</sup> Polyglutamine (Q42)

Antibody	Origin	Antibody construct	Binding capacity	Epitope	Main results	Additional comment	Ref.
<b>5. Camelid antibodies</b>							
<b>KW1(AP)</b>	Recombinant, selected against immobilized A $\beta$ 40 oligomers through competition with monomers from a synthetic camelid phage display library generated in house.	One heavy chain domain only (VHH-domain/ nanobody), ~15 kDa.	Binds A $\beta$ 40 oligomers. Do not recognize monomers or fibrils. Distinguishes between different types of oligomers.	Conformational. Recognizes oligomers through a hydrophobic and significantly aromatic surface motif that includes residues 18–20.	Prevents the formation of fibrils and allows non-fibrillar aggregates to prevail. Do not disaggregate preformed A $\beta$ fibrils significantly.	Same research group as B10.	87
<b>B10(AP)</b>	Recombinant, selected against A $\beta$ 40 fibrils from a synthetic camelid phage display library generated in house.	One heavy chain domain only (VHH-domain/ nanobody), ~15 kDa.	Binds A $\beta$ 40 fibrils, not monomers. Also bind amyloid fibrils from A $\beta$ 42, AA <sup>15</sup> and Ig V <sub>L</sub> .	Conformational. Competition between AA and Ig V <sub>L</sub> suggest that B10 binds the same structural region.	Prevents the formation of A $\beta$ 40 fibrils, but do not disaggregate preformed. ~1/3 of the CDR residues possesses basic properties, and mutagenesis and x-ray crystallography imply that their specificity depend on electrostatic interactions to an acidic moiety common to different amyloid fibrils. One B10 binds ~seven A $\beta$ 40 molecules.	Same research group as KW1.	88,89
<b>V31-1</b>	Recombinant selected from a Camelid phage display library generated in house from VHH raised in alpaca against A $\beta$ 42.	One heavy chain domain only (VHH-domain/ nanobody), ~15 kDa.	Bind monomers and oligomers	C-terminal	Inhibits A $\beta$ 42 aggregation and cytotoxicity.	Reported on additional 3 scFv's but focused on V31-1, which had highest affinity.	90

Antibody	Source	Antibody construct	Binding capacity	Epitope	Main results	Additional comment	Ref.
<b>6. Special antibody formats</b>							
<b>Gamma-bodies<sup>16</sup></b>	Recombinant, 6-10 residues long peptides of A $\beta$ 42 are grafted into CDR3 producing 12 different gammabodies.	V <sub>H</sub> antibody, ~15 kDa	V <sub>H</sub> 's displaying: <b>A<math>\beta</math>12–21, 15–24, and 18–27</b> recognise fibrils; <b>C-terminus</b> recognise all three A $\beta$ conformers; and <b>N-terminus and between the amyloidogenic motifs</b> do not recognise A $\beta$ .	The amino acid sequence (instead of the amino acid composition) of the grafted A $\beta$ motifs mediates antibody binding.	The antibodies recognising A $\beta$ oligomers and fibrils inhibit toxicity.	Hypothesis: grafting peptides containing amyloidogenic segments ( <sup>17</sup> LVFFA <sup>21</sup> and <sup>30</sup> AIIGLMVGGVVIA <sup>42</sup> ) would mediate antibody recognition of aggregated A $\beta$ conformers, whereas grafting A $\beta$ segments outside these regions would not.	91
<b>HIRMAB-ScFv</b>	Fusion antibody consisting of two scFv's directed against A $\beta$ 1-28, one HIRMAB <sup>17</sup> and one constant region of an IgG.	Murine scFv, chimeric (human and murine) HIRMAB delivery antibody and constant region of monoclonal human IgG1, ~200 kDa.	Soluble A $\beta$ 40 and A $\beta$ 40 fibrils as well as the HIR	N-terminal	It crosses the blood brain barrier (BBB) bidirectionally. The scFv's causes disaggregation of fibrils.	Fusion antibody of a delivery antibody (HIRMAB) that binds to the HIR and mediates brain uptake and therapeutic scFv's	92

<sup>16</sup> Grafted amyloid-motif antibodies

<sup>17</sup> Monoclonal antibody genetically engineered to the human insulin receptor (HIR)

**Table S2.** Amino acid sequences of the heavy ( $V_H$ ) and light ( $V_L$ ) chain regions of the identified scFvs that selectively inhibit secondary nucleation (I2, I48, J44 and J57), and of those that may also inhibit elongation (I68, J7, J46). Between  $V_H$  and  $V_L$  there is a  $S_2G_4SG_4S_2$  linker in all scFvs. Color codes: green hydrophilic, yellow hydrophobic, red negatively charged, blue positively charges, grey no side-chain. For J46, the variable regions of  $V_H$  contained double sequences, even after retransformation and selection of multiple single colonies. Therefore, J46 may represent two scFvs in the same plasmid that have the same light chain sequence, and we show here the amino acids resulting from strongest signal.

### $V_H$

Clone	Fr1	CDR1	Fr2	CDR2	Fr3	CDR3	Fr4
				* * * * *		* * * * *	
I2	EVQLLES GGG L V Q P G G S L R L S C A A S G F T F S	SYAMS	WVRQAPGKGLEWVS	XI <b>YNY</b> G Y T T N YADSVKG	RFTISRDN SKNTLYLQ MNSLRAEDTAVYYCAK	<b>TAY</b> GFDY	WGQGLTVTVSS
I48	EVQLLES GGG L V Q P G G S L R L S C A A S G F T F S	SYAMS	WVRQAPGKGLEWVS	<b>GINTT</b> G S N T YADSVKG	RFTISRDN SKNTLYLQ MNSLRAEDTAVYYCAK	<b>SDS</b> GFDY	WGQGLTVTVSS
J44	EVQLLES GGG L V Q P G G S L R L S C A A S G F T F S	SYAMS	WVRQAPGKGLEWVS	<b>A</b> I N K G G Y K T YADSVKG	RFTISRDN SKNTLYLQ MNSLRAEDTAVYYCAK	<b>TPK</b> GFDY	WGQGLTVTVSS
J57	EVQLLES GGG L V Q P G G S L R L S C A A S G F T F S	SYAMS	WVRQAPGKGLEWVS	<b>A</b> I N K G G Y K T YADSVKG	RFTISRDN SKNTLYLQ MNSLRAEDTAVYYCAK	<b>TPK</b> GFDY	WGQGLTVTVSS
I68	EVQLLES GGG L V Q P G G S L R L S C A A S G F T F S	SYAMS	WVRQAPGKGLEWVS	<b>GIDYT</b> G T S T A YADSVKG	RFTISRDN SKNTLYLQ MNSLRAEDTAVYYCAK	<b>SDN</b> GFDY	WGQGLTVTVSS
J7	EVQLLES GGG L V Q P G G S L R L S C A A S G F T F S	SYAMS	WVRQAPGKGLEWVS	<b>TIKSK</b> G N H T V YADSVKG	RFTISRDN SKNTLYLQ MNSLRAEDTAVYYCAK	<b>RNR</b> GFDY	WGQGLTVTVSS
J46	EVQLLES GGG L V Q P G G S L R L S C A A S G F T F S	SYAMS	WVRQAPGKGLEWVS	<b>TI</b> S N X G V Q T X YADSVKG	RFTISRDN SKNTLYLQ MNSLRAEDTAVYYCAK	<b>RLHR</b> GFDY	WGQGLTVTVSS

### $V_L$

Clone	Fr1	CDR1	Fr2	CDR2	Fr3	CDR3	Fr4
				* *		* * * * *	
I2	DIQMTQSPSSLSASVGDRTITC	RASQSISSYLN	WYQQKPGKAPKLLIY	<b>N</b> A S T L Q S	GVPSRFSGSGSGTDFTLTISLQPEDFATYYC	QQ <b>NNSS</b> P T	FGQGTKVEIKRAA
I48	DIQMTQSPSSLSASVGDRTITC	RASQSISSYLN	WYQQKPGKAPKLLIY	<b>D</b> A S S L Q S	GVPSRFSGSGSGTDFTLTISLQPEDFATYYC	QQ <b>SNAT</b> P A T	FGQGTKVEIKRAA
J44	DIQMTQSPSSLSASVGDRTITC	RASQSISSYLN	WYQQKPGKAPKLLIY	<b>R</b> A S R L Q S	GVPSRFSGSGSGTDFTLTISLQPEDFATYYC	QQ <b>QNR</b> T P R T	FGQGTKVEIKRAA
J57	DIQMTQSPSSLSASVGDRTITC	RASQSISSYLN	WYQQKPGKAPKLLIY	<b>G</b> A S V L Q S	GVPSRFSGSGSGTDFTLTISLQPEDFATYYC	QQ <b>ANTK</b> P A T	FGQGTKVEIKRAA
I68	DIQMTQSPSSLSASVGDRTITC	RASQSISSYLN	WYQQKPGKAPKLLIY	<b>T</b> A S A L Q S	GVPSRFSGSGSGTDFTLTISLQPEDFATYYC	QQ <b>YNNG</b> P A T	FGQGTKVEIKRAA
J7	DIQMTQSPSSLSASVGDRTITC	RASQSISSYLN	WYQQKPGKAPKLLIY	<b>S</b> A S L Q S	GVPSRFSGSGSGTDFTLTISLQPEDFATYYC	QQ <b>Q</b> Q K Y P P T	FGQGTKVEIKRAA
J46	DIQMTQSPSSLSASVGDRTITC	RASQSISSYLN	WYQQKPGKAPKLLIY	<b>R</b> A S L Q S	GVPSRFSGSGSGTDFTLTISLQPEDFATYYC	QQ <b>RGHS</b> P P T	FGQGTKVEIKRAA

**Table S3. The difference between the Tomlinson scFv libraries.** Both the I and J library have diversified side chains at 18 positions within the CDR regions. Those 18 residues are H50, H52, H52a, H53, H55, H56, H58, H95, H96, H97, H98, L50, L53, L91, L92, L93, L94 and L96, where H and L corresponds to the heavy respectively light chain. The table shows which nucleotides are possible in the three positions in the degenerate codons of each library, using standard degenerate base nomenclature D=G/A/T, V=G/C/A, K=G/T and N=G/C/A/T. In the Tomlinson I library, the varied amino acid positions may contain Cys, Asp, Asn, Thr, Ser, Tyr, Gly or Ala, while in the Tomlinson J library all 20 amino acids are possible.

Position in codon	Tomlinson I		Tomlinson J	
	Degenerate base	Possible nucleotides	Degenerate base	Possible nucleotides
1	D	G, A, T	N	G, C, A, T
2	V	G, C, A	N	G, C, A, T
3	T	T	K	G, T